Article:
Wang, Q, Yang, S, Glover, PWJ orcid.org/0000-0003-1715-5474 et al. (3 more authors) (2020) Effect of Pore-Throat Microstructures on Formation Damage during Miscible CO2 Flooding of Tight Sandstone Reservoirs. Energy & Fuels, 34 (4). pp. 4338-4352. ISSN 0887-0624

https://doi.org/10.1021/acs.energyfuels.0c00158

Effect of pore-throat microstructures on formation damage in tight sandstone reservoirs during miscible CO2 flooding

Journal:	*Energy & Fuels*
Manuscript ID	ef-2020-00158a.R1
Manuscript Type:	Article
Date Submitted by the Author:	27-Feb-2020
Complete List of Authors:	Wang, Qian; China University of Petroleum Beijing, Yang, Shenglai; China University of Petroleum-Beijing, Beijing, Lorinczi, Piroska; University of Leeds Glover, Paul; University of Leeds QIAN, KUN; China University of Petroleum Beijing

Effect of pore-throat microstructures on formation damage during miscible CO_2 flooding of tight sandstone reservoirs

Qian Wang[1, 2], Shenglai Yang[1]*, Paul W.J. Glover[2], Piroska Lorinczi[2], Kun Qian[1]

1 School of Petroleum Engineering, China University of Petroleum-Beijing, Beijing 102249, China
2 School of Earth and Environment, University of Leeds, Leeds, LS2 9JT, UK
*Correspondence: yshenglai820@163.com

Abstract: Pore and throat blockage as well as wettability alteration caused by asphaltene deposition are serious problems during injection of CO_2 into subsurface reservoirs for Enhanced Oil Recovery (EOR). During miscible CO_2 flooding, the efficacy and distribution of fluid flow in sandstone reservoirs is controlled by the pore-throat microstructure of the rock. Furthermore, CO_2 injection promotes asphaltene precipitation on pore surfaces and in the pore-throats, decreasing the permeability and altering reservoir wettability. In this work, miscible CO_2 flooding experiments under reservoir conditions (up to 70±0.1°C, 18 MPa) have been carried out on four samples with very similar permeabilities but significantly different pore size distributions and pore-throat structures in order to study the effects of pore-throat microstructure on formation damage. The features of pore-throat structure were evaluated by fractal theory, based on constant-rate mercury intrusion (CRMI) tests. Reservoir rocks with smaller pore-throat sizes and more heterogeneous and poorer pore-throat microstructures were found to be more sensitive to asphaltene precipitation, with corresponding 14-22% lower oil recovery factors (RFs) and 4-7% greater decreases in permeability compared to more homogeneous rocks and rocks with larger pore-throats. However, the water-wettability index of cores with larger and more connected pore-throat microstructures was found to drop by an extra 15-25% compared to the water wettability decrease found for heterogeneous cores. We attribute these observations to an increase in asphaltene precipitation caused by the larger sweep volume of injected CO_2 which occurs in rocks with larger and more homogeneous pore-throats. In addition, we observed that rocks with more homogeneous pore-throat microstructures also exhibit homogeneity in the consequent distribution of formation damage.

Keywords: CO_2 flooding, pore-throat microstructure, asphaltene precipitation, permeability decline, and wettability alteration, Changqing oilfield

Introduction

The development of unconventional reservoirs has contributed significantly to the growth of global oil production. Tight sandstone reservoirs have played an important role in unconventional oil production. Such reservoirs are typically characterised by poor reservoir quality and well-developed spatial heterogeneity, often in multiple directions. The consequent variable and relatively high water saturations make them difficult to develop [1-2].

Flooding with CO_2 is a reliable and common EOR strategy which has been used widely in a significant number of tight sandstone reservoirs [3-6]. The major CO_2-EOR mechanisms include (i) miscible and immiscible displacement, (ii) interfacial tension (IFT) reduction, (iii) oil viscosity reduction, (iv) the so-called oil-swelling effect, and (v) light-hydrocarbons extraction by supercritical CO_2 [7-10]. Compared with the high efficiency of miscible CO_2 flooding, immiscible CO_2 flooding in reservoirs can easily cause an early CO_2 breakthrough (BT) and a low oil RF. The most important factor that affects CO_2 displacement efficiency is the minimum miscibility pressure (MMP) of the crude oil–CO_2 system at actual reservoir conditions [11-13].

However, when CO_2 is injected in reservoirs and is in contact with crude oil, variations in composition of the crude oil due to the dissolved CO_2 can cause asphaltenes to deposit from crude oil and flocculate into asphaltene precipitation particles [14-16]. The asphaltene solid particles are captured at pore-throats and adsorbed on the pore surfaces, resulting in blocked pores and pore-throats, and consequent wettability alteration [17-18]. The blockages of the pore-throats damage the reservoir by reducing its permeability, which makes CO_2 injection more difficult. Adsorption of asphaltene to pore surfaces also changes the wettability of the rock, making the rock less water-wet and more oil-wet. The transition of reservoir wettability to oil-wet makes it more difficult for crude oil in the pores to be displaced, resulting in high residual oil, and immediate reductions in productivity and increases in water cut [19-20].

Fractal theory is an effective method for investigating physical properties of rocks [21]. This approach builds a bridge between micro-morphology (pore size and shape, pore size distribution, pore connectivity) and parameters which control macroscopic performance (porosity, permeability), while allowing the characterisation of the complexity and irregularity of pore-throat structures [22]. Fractal geometry has been successfully used to characterize the spatial heterogeneities of different patterns over a wide range of pore spaces in sedimentary rocks [23-26] .

The processes of fluid transport through underground reservoirs and the resulting instantaneous and final distributions of fluid in the pores and throats of the rocks during the CO_2 flooding process are controlled strongly by the pore microstructure, and particularly by the distribution of pore-throat sizes. Consequently, the pore microstructure and pore-throat size distributions are important factors affecting crude oil recovery [27]. There are a number of different ways that varying pore-throat structures may

lead to different oil recovery factors and residual oil distributions. First, rocks with a more heterogeneous pore-throat microstructure are more sensitive to fingering, which leads to inefficient CO_2 flooding and larger residual oil saturations [28-29]. Second, pore-throat distributions control fluid flow and hence the migration, deposition and adsorption of asphaltene particles. Consequently, asphaltene deposition is controlled by pore-throat size distribution and heterogeneity, but also affects the pore-throat size distribution and heterogeneity by the asphaltene particles themselves blocking pore-throats [30]. Third, heterogeneity in fluid flow caused by heterogeneity in the pore-throat size distribution causes heterogeneity in asphaltene adsorption to pore surfaces, resulting in heterogeneity in the wettability of the rock. Consequently, different pore microstructures will have different sensitivities to damage caused by asphaltene precipitation [31]. Therefore, effects of pore-throat structure on reservoir blockage and wettability alteration during CO_2 injection are complex, interrelated and worthy of further study.

Extensive core-flooding experiments have been conducted in order to investigate permeability decline and wettability alteration caused by asphaltene precipitation during CO_2 flooding processes [32-34], including the effects of permeability, displacement pressure, displacement methods, crude oil properties and other factors on asphaltene precipitation and reservoir damage [35-39]. In addition, the distributions of blockage by asphaltene precipitation in the pores and throats of sandstone have been evaluated quantitatively using nuclear magnetic resonance (NMR) measurements [14, 40]. Nevertheless, the effects of the rock pore-throat structure on the damage to pore-throat structure itself during asphaltene precipitation have been rarely studied directly [35, 41]. In previous work, it has been recognised that core permeability has an influence on displacement pressure and fluid seepage during the displacement process. Consequently, similar initial call permeabilities and the accurate evaluation of pore-throat structure are both important prerequisites for experimental research, if other influences are to be studied effectively. Unfortunately, these prerequisites have not been satisfied in most core-flooding experiments [32, 42]. In addition, while the distributions of pore-throat blockage have been studied qualitatively through the distributions of oil and water re-saturation after flooding in previous studies, the influences of wettability alteration have been ignored [14, 40].

In this work, the influences of pore-throat structure on the variations in petrophysical properties of cores have been studied, and the distribution of these changes are analysed quantitatively. Four core plugs with comparable permeability but significantly different pore size distributions were selected and measured using Constant-Rate Mercury Intrusion (CRMI) tests. The pore-throat structure of each of the four cores was evaluated by fractal theory from the Mercury Injection Capillary Pressure (MICP) curves [21, 43]. A set of miscible CO_2 core-flooding experiments was carried out on the cores at the reservoir temperature (70±7°C) and reservoir pressure (18±1.5 MPa, >MMP). The post-flood oil recovery factor (RF), component variation and residual oil distribution were all measured. The permeability decline, wettability variation and distribution of variations in petrophysical properties were compared by monitoring variations in gas permeability, Amott-Harvey indexes, and Nuclear Magnetic

Resonance (NMR) transverse relaxation time (T_2) spectra, before, during and after core-flooding. These results can be used to evaluate the extent of changes in the reservoir pore-throat microstructure as a result of CO_2 flooding. Consequently, measures to minimize the impact of reservoir damage caused by asphaltene precipitation on crude oil recovery have been considered, discussed and recommended.

Methodology

Materials

The experimental core flooding reported in this work used fluids which were based upon those from the Changqing oilfield, in the Ordos Basin of western China. The reservoir is predominantly sandstone and lies at a depth of 2100-2400 m. The core flooding used synthetic live oil (Table 1), which was prepared in the laboratory to match the field sample. In order to do this, the composition of the live oil was measured by gas chromatography (Table 2). The content of the asphaltene component (*n*-C5 insoluble) of the crude oil was measured to be 1.32 wt% using the standard ASTM D2007-03 method. Asphaltenes begin to precipitate in crude oil at 9.6 MPa at these reservoir conditions, as noted in our previous experiments (Wang et al., 2020 in press). The relationship between CO_2 concentration in crude oil and asphaltene precipitation (Figure 1) can be predicted based on the Flory-Huggins model [44]. The purity of CO_2 used in this study was 99.99%. Two types of formation water were used in the experiments. One was an ordinary brine which was prepared according to the composition given in Table 3, the other was made in the same way but Mn^{2+} was added. The brine containing Mn^{2+} was used to screen the water signal during NMR tests in order to obtain only the oil distribution in the core [14].

Table 1. Basic physical properties of live oil.

Items	Live oil
Density (g/cm^3)	0.725±0.002 (70°C)
Viscosity (cP)	3.88±0.05 (70°C)
Solution gas-oil ratio (m^3/m^3)	31.4
Bubble point pressure (MPa)	7.52

Table 2. Compositional analysis result of the live oil (*n*-C5 insoluble asphaltene content =1.32 wt%).

Carbon number	wt%	Carbon number	wt%	Carbon number	wt%
CO2	0.08	C9	6.46	C21	1.80
N2	0.31	C10	5.70	C22	1.92
C1	1.50	C11	4.86	C23	1.67
C2	0.60	C12	4.21	C24	1.74

C3	0.49	C13	4.28	C25	1.59
iC4	0.25	C14	4.45	C26	1.56
nC4	0.47	C15	3.88	C27	1.58
iC5	1.18	C16	3.38	C28	1.48
nC5	0.22	C17	3.08	C29	1.40
C6	4.86	C18	2.93	C30+	15.78
C7	5.55	C19	2.38	**Total**	**100**
C8	6.10	C20	2.28		

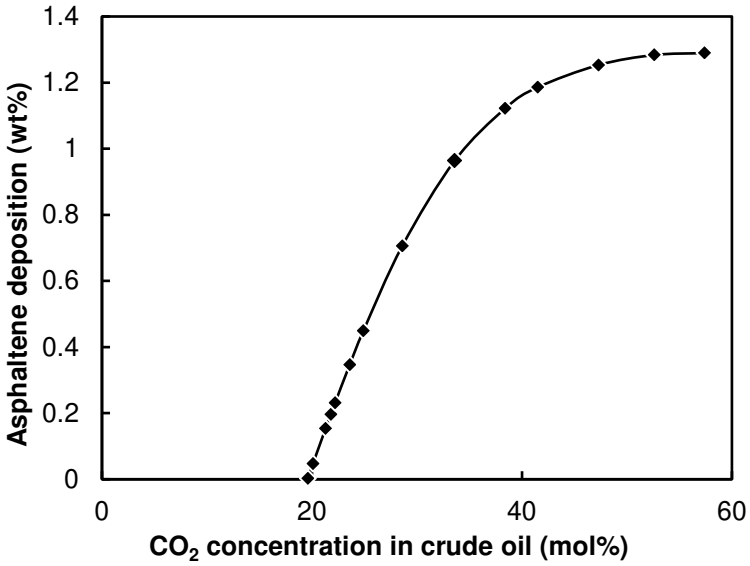

Figure 1. Effect of CO_2 on the amount of asphaltene deposition (wt%) at P=18 MPa and T=70 °C. Uncertainties in the x and y directions are smaller than the symbol size in all cases[17].

Table 3. Physicochemical properties of the reservoir brine.

Item	Value
Density (g/cm^3)	1.01
Viscosity at 25°C (cP)	1.03
pH	7.04
K^+ (mg/L)	296
Na^+ (mg/L)	3494
Ca^{2+} (mg/L)	7134
Mg^{2+} (mg/L)	48.2
Cl^- (mg/L)	18433
SO_4^{2-} (mg/L)	114
TDS (mg/L)	29520

A group of 19 cores with similar permeability values were selected from 237 core samples, which were obtained from the Changqing reservoir. The selected cores were saturated with brine under vacuum for

24 hours and were measured by NMR apparatus to obtain a T_2 distribution for each core. The shape of the T_2 distribution of 19 samples exhibits 4 of the 5 typical T_2 distributions that are observed in Changqing reservoir rocks [45]. A subset of 4 cores were selected from the 19 cores to represent the 4 typical T_2 distributions; numbered H1, H2, H3 and H4 (Figure 2, Table 4).

Porosity and permeability measurements were made on the four cores. The calculated uncertainties in porosity measurements are <3%, while uncertainties in the permeability measurements are about 4%. After the cores were cleaned and dried, the cores were cut to a length of 5 cm, and the offcuts were analysed by X-ray diffraction (XRD, Model: D8 Focus, Bruker, MA, USA) to obtain the mineral content of each core (Table 5).

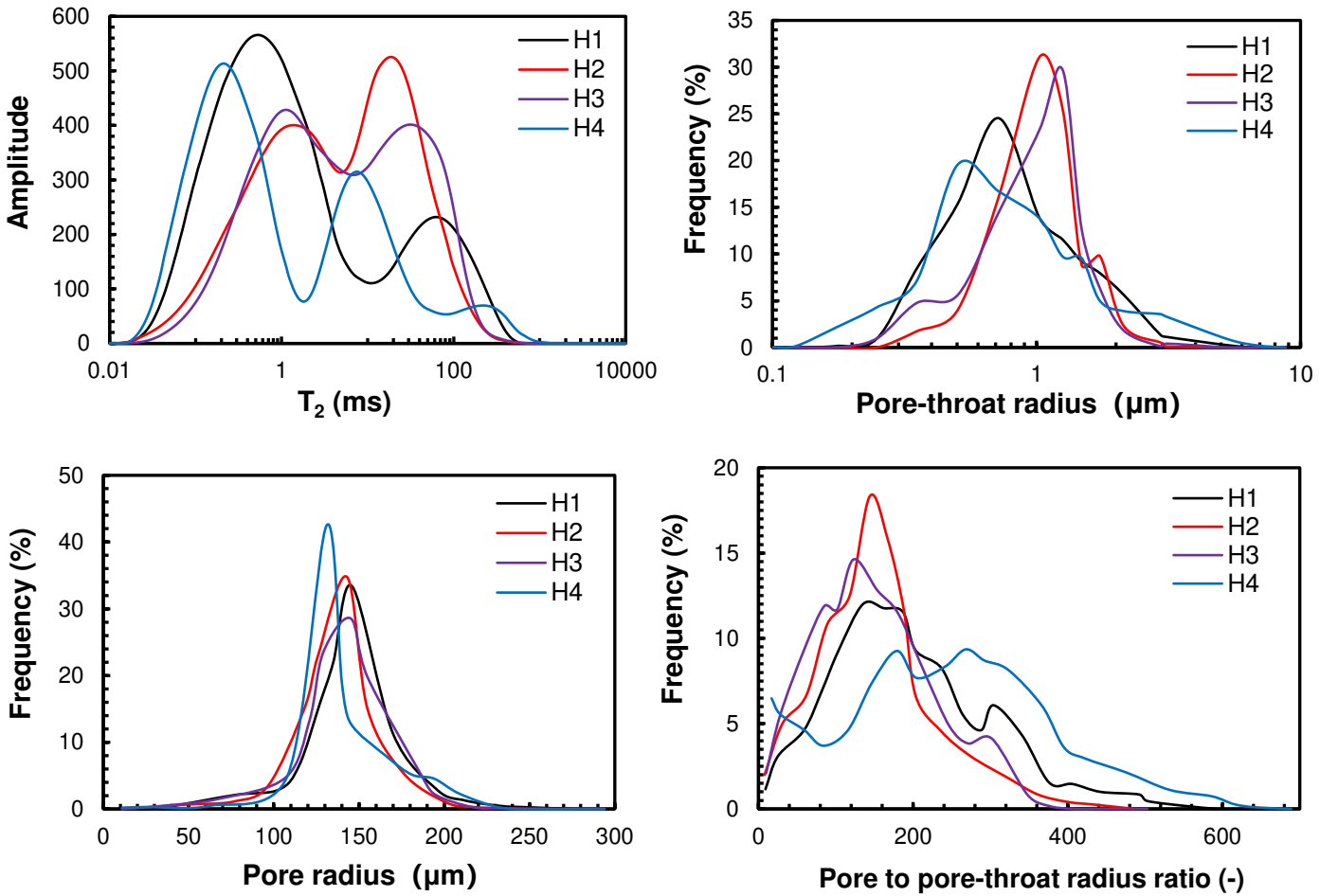

Figure 2. NMR and CRMI results before experiments. The upper left panel shows the T_2 spectrum of four cores in fully saturated brine before experiments obtained by NMR tests, reflecting the pore size distribution of the four cores. The other three graphs are the distributions of throat radius, pore radius and the pore-throat ratio before experiments according to the results of CRMI tests.

Table 4. Basic parameters of the core samples, and CRMI-derived fractal dimensions.

Core number	Length (cm)	Diameter (cm)	Permeability (mD)	Porosity (%)	Fractal dimension
H1	5.11	2.54	0.713	14.62	2.706
H2	5.07	2.54	0.742	14.14	2.622
H3	5.09	2.53	0.769	13.62	2.596
H4	5.02	2.54	0.734	11.85	2.748

Table 5. Types and contents of mineral in the cores.

Core number	Mineral types and content (wt%)						
	Quartz	K-feldspar	Plagioclase	Calcite	Dolomite	Clay minerals	Others
H1	45.7	9.5	37.1	1.3	0.9	4.4	1.1
H2	42.6	12.9	33.9	4.1	1.1	2.9	2.5
H3	48.9	8.6	29.9	5.2	1.8	3.7	1.9
H4	39.7	16.1	32.1	2.8	2.3	4.3	2.7

NMR Measurements

The Nuclear Magnetic Resonance (NMR) apparatus (Mini-MR, Niumag, Suzhou, China) used in this study detects the transverse relaxation motion of hydrogen nuclei of fluids in the pores to obtain the T_2 spectrum, which represent the distribution of fluids in pores [40]. The frequency range, magnetic intensity and magnetic intensity gradient of the NMR apparatus are 1-30 MHz, 0.5 T, and 0.025 T/m, respectively, the precision in the frequency control is 0.01 MHz. For each core NMR scanning is repeated three times to confirm the repeatability of the measurement. In our work, the range 0.1-10 ms of T_2 was considered to represent small pores, while relaxation times in the range 10-1000 ms were considered to represent large pores.

Mercury Injection Capillary Pressure

A set of CRMI measurements were conducted using an APSE-730 mercury porosimeter (American Coretest Systems, Inc.) to obtain the MICP characteristics of the samples. The CRMI measurements were executed at a quasi-static constant speed of 50 nL/min. Pore body and pore-throat size distributions were obtained from fluctuations in the capillary pressure [46] (Figure 2). The total MICP curve could be partitioned into two curves, representing the pore body capillary pressure curve and the pore-throat capillary pressure curve. Four small samples obtained by dividing the four cores were measured, and the radius of pores and pore-throats, as well as the pore to pore-throat ratio were obtained. The maximum injection pressure of the CRMI is 6.2 MPa to keep the intrusion rate quasi-static, the corresponding pore radius is approximately 0.12 μm.

Fractal features

The pore-throat structure of reservoir rocks with fractal features can be characterized quantitatively by defining a fractal dimension [22-24]. The capillary pressure is usually given as

$$P_c = \frac{2\sigma cos\theta}{r}, \quad \textbf{(1)}$$

where, P_c *is* the capillary pressure (MPa), σ is the interfacial tension (N/m), θ is the contact angle, and r is the pore radius (μm).

The relationship between capillary force and wetting saturation can be written as[21],

$$logS = (D-3)\log P_c + (3-D)\log P_{min}, \quad \textbf{(2)}$$

where, S (fractional) is the saturation of the wetting phase corresponding to the capillary pressure, P_c (MPa), D is the fractal dimension (unitless), and P_{min} is the capillary pressure corresponding to the largest pore-throat (MPa).

A linear relationship exists between the logarithm of the capillary pressure and the corresponding logarithm of the saturation of the wetting phase (mercury is the non-wetting phase). Consequently, the CRMI test results can be subjected to linear regression analysis in order to obtain the pore fractal dimension D for drainage. This value can be used to characterize the pore-throat structure. According to the fractal theory, the fractal dimension in the three-dimensional Euclidean space is between 2 and 3. The upper value 3 corresponds to a totally irregular or rough surface, whereas the lowest value 2 corresponds to a perfectly smooth pore surface and regular pore shape [24-26]. The value of fractal dimension is a representation of rock heterogeneity, it increases continuously as the complexity of pore network increases. In other words, the greater the fractal dimension, the greater heterogeneity of pore-throat structure. Consequently, fractal dimension can be used to describe quantitatively the homogeneity of pore-throat structure, as we have done in this paper. The values derived from the fractal analysis for each of the cores used in this paper are given in Table 4.

Wettability Measurements

In this study, the Amott-Harvey wettability index is used to assess the overall average wettability of the cores. The Amott-Harvey wettability index is a measure of the macroscopic mean wettability of a rock to a given fluid. It involves the measurement of the amount of fluids spontaneously and forcibly imbibed by rock sample. It has no validity as an absolute measurement, and does not indicate how wettability might vary at a microscopic scale, but it is industry standard for comparing the wettability of various core plugs [47]. Since the Amott-Harvey index is a macroscopic measurements of wettability, it cannot distinguish between an intermediate wettability system and a mixed wettability system.

It is worth noting that before each wettability test, the cores should be aged in brine for 24 hours to eliminate the influence of the wettability differences between cores on the experimental results, while eliminating the impact of process of oil saturation and CO_2 flooding on the wettability, and only keeping

the impact of asphaltene precipitation adsorbed on the pore surface on the wettability of rocks. The dry cores were evacuated and then saturated with oil. The cores were then immersed in brine in a standard imbibition cell for at least 48 h, during which the volume of oil displaced by spontaneous imbibition of brine was recorded. Subsequently, the core was centrifuged under brine with capillary pressure of -25 psi (-0.172 MPa). The volume of oil displaced by forced imbibition of brine was recorded. The Amott water index was calculated as follows,

$$\delta_w = \frac{V_{si}}{(V_{si}-V_{fi})} , \quad \textbf{(3)}$$

where, V_{si} is the oil volume displaced by spontaneous imbibition of brine (ml), and V_{fi} is the oil volume displaced by forced imbibition of brine (ml).

The Amott oil index is similarly measured,

$$\delta_o = \frac{V_{sd}}{(V_{sd}-V_{fd})} , \quad \textbf{(4)}$$

where, V_{sd} is this the water volume by spontaneous drainage of oil (ml), and V_{fd} is the water volume (ml) by forced drainage of oil by centrifuging with a capillary pressure of +100 psi (+0.689 MPa).

The Amott-Harvey index is then calculated as follows,

$$\delta_{AH} = \delta_w - \delta_o . \quad \textbf{(5)}$$

The value of δ_{AH} measured by this method is between -1 and 1. The closer the index is to 1, the stronger the average water wetness of the rock. The closer the index is to -1, the stronger the average oil wettability.

The MMP Test

The slim-tube apparatus (CFS-100, Core Lab, Tulsa, OK, USA) shown in Figure 3 was used to measure the MMP of the crude oil-CO_2 system. The apparatus consisted of a stainless steel slim tube packed with silica sand (Shengfa Mining Industry Co. Ltd., China), a dual displacement pump (260D, ISCO, Lincoln, NE, USA), a back-pressure regulator (Huada, China) and two pressure transducers to monitor injection pressure and back pressure constantly. A gas flow meter was used to measure the volume of the produced gas, a burette was used to collect and measure the produced oil.

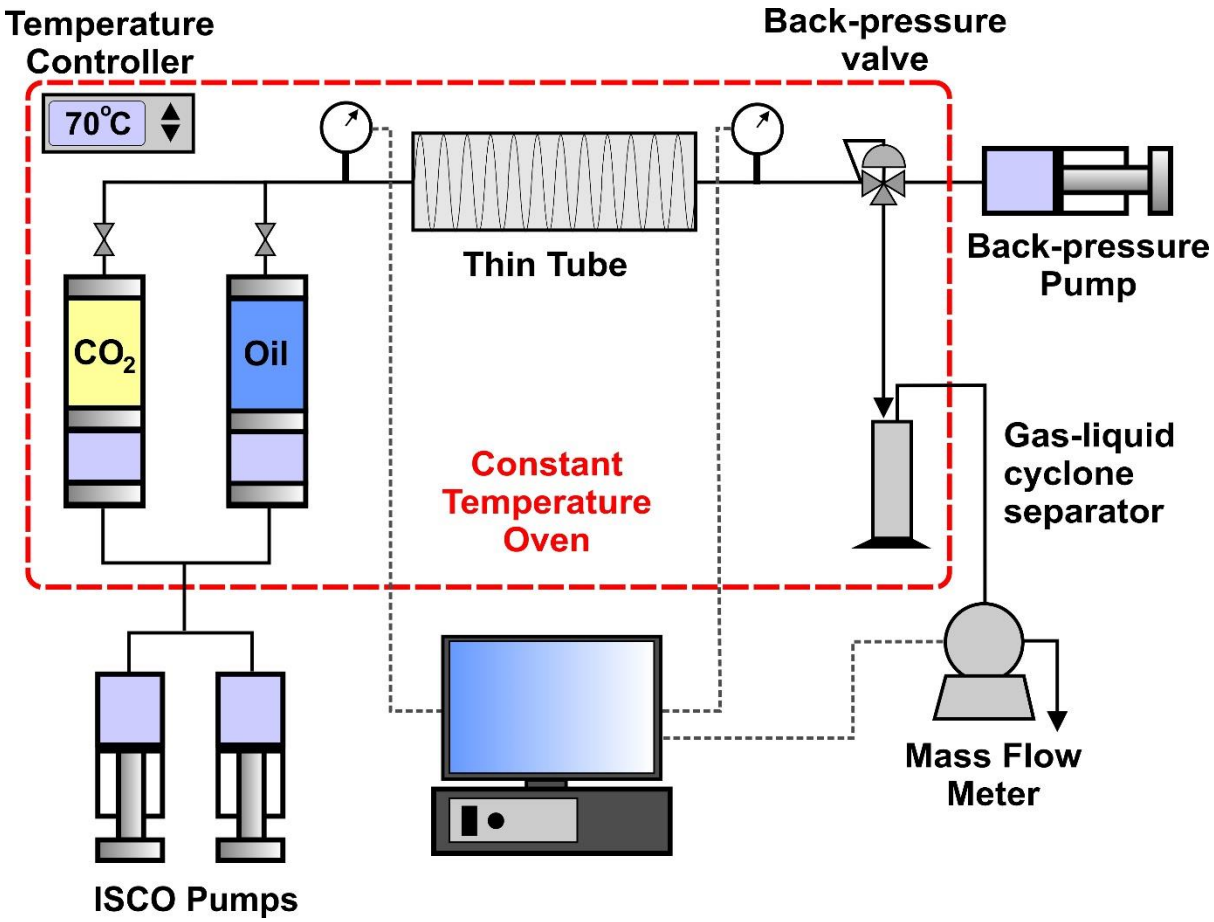

Figure 3. Schematic diagram of the slim-tube apparatus.

Seven slim-tube tests with different pressures, but all at a temperature of 70±0.1°C, were carried out. The displacement system was cleaned using petroleum ether and dried by nitrogen, after which the apparatus was fully saturated with crude oil while the back pressure was maintained at the desired production pressure in order to prevent the crude oil from degassing. The CO_2 was injected into the slim tube to displace the crude oil with a constant flow rate of 0.1 cm^3/min at the set injection pressure. The injection and production pressure was continuously monitored and recorded during the entire experiments. The volume of the produced oil and gas was measured at every 0.1 pore volume (PV) of injected CO_2 until 1.2 PV of CO_2 had been injected.

Core-flooding tests

A schematic diagram of high-pressure core flooding apparatus used for CO_2 flooding experiments is shown in Figure 4. Brine, live oil, brine with $MnCl_2$ (Mn^{2+}, 15000 mg/dm^3), and CO_2 were contained separately in four high pressure cylinders (Hongda, China; P=80 MPa; T=130°C). A dual ISCO syringe pump was used to inject the crude oil, formation water or CO_2 from the high pressure cylinders to the core holder (Hongda, China; P=80 MPa; T=130°C), which is a special core holder, compatible with the NMR spectrometer. A pump was used to maintain confining pressure, and another pump and a back

pressure valve were used together to regulate and maintain the back pressure. The cylinders and core holder were placed in the constant temperature oven (Hongda, China; T=150.0°C) with the temperature being regulated within ±0.1°C by the temperature controller. The produced brine, oil and gas were collected and quantified by a gas-liquid cyclone separator and a mass flow meter. Flow data and pressure were logged automatically by computer during the experiments.

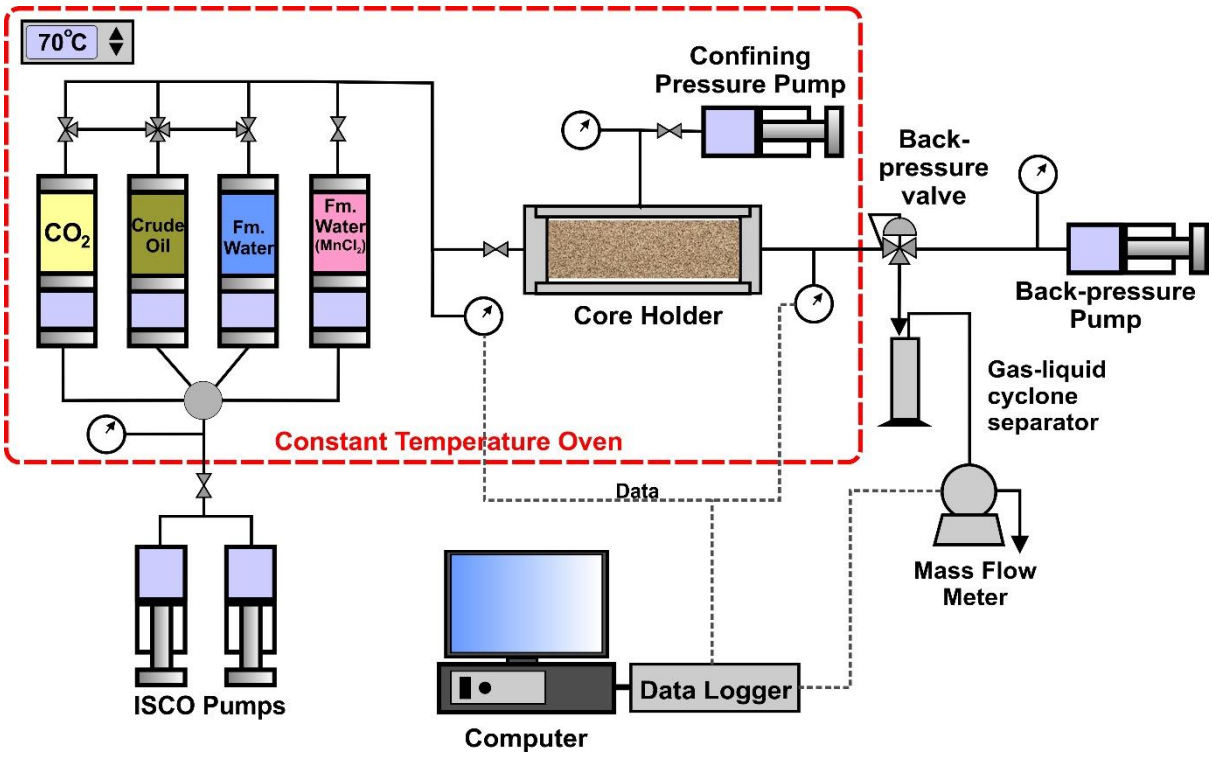

Figure 4. Schematic diagram of the miscible CO_2-WAG core-flood apparatus.

The core-flooding procedure are described as follows.

(1) The constant temperature oven was raised to 70±0.1°C and held at that temperature for 24 hours. The core was inserted into the core holder after being cleaned and dried, followed by being evacuated and saturated with ordinary brine. The NMR apparatus was then used to measure T_2 spectrum of the brine in core sample at initial water-saturated conditions. The core was displaced with the $MnCl_2$ enriched brine for 5 PV. The saturated core was then rescanned by the NMR apparatus to make sure the signal of the brine had been eliminated.

(2) The crude oil was injected into the core, the oil injection was stopped after 30 hydrocarbon pore volumes (HCPV) in order to achieve an initial oil saturation (S_{oi}) and connate water saturation

(S_{wc}). The core holder was left undisturbed for at least 24 hours to attain an equilibrium condition at 70±0.1°C and 18 MPa. The T_2 spectrum of oil in the core was then measured again.

(3) In each test, CO_2 was injected with a constant flow rate of 0.02 cm^3/min into the core-holder to displace the crude oil. The pressure at the outlet of the core holder was maintained at 18 MPa. Each core-flood was stopped when no more oil evolved from the core and each core was injected with the same volume of CO_2. The volumes of injected and produced fluid, the injection and production pressures were recorded continuously throughout the entire flooding experiment. The core in the core holder was then re-tested by NMR to obtain the distribution of the residual oil in the core. The produced oil was collected during each core-flood test, and the asphaltene content in the produced oil were analyzed.

Post-flooding tests

Asphaltene is soluble in aromatics but not in alkanes. Consequently, all organic components of oil except asphaltene could be cleaned from the core by extraction with *n*-heptane [46] using a Soxhlet extractor (SXT-02, Shanghai Pingxuan Scientific Instrument CO., Ltd., China). Subsequently, the cores were dried and their porosity and gas permeability were measured. Since the extraction process left asphaltene precipitation in place, these measured porosities and gas permeabilities are those which are affected by asphaltene precipitation. In order to reduce experimental errors, three measurements of porosity and gas permeability were always measured, with the reported value being the arithmetic mean of all three.

In order to study the distribution of core petrophysical property variations with the effect of asphaltene precipitation, the cores were immersed in brine for 24 hours for aging to eliminate the impact of saturated oil on wettability variations. The cores were then subjected to the same treatments as described from Step 1 to Step 2, above, in order to obtain the distribution of re-saturated brine and oil in cores. Subsequently, the cores were cleaned and aged by brine again to remove the effects of saturated oil, then were tested to elicit how wettability had been affected by asphaltene precipitation.

Samples were taken from the cores for CRMI tests to obtain the MICP of cores containing asphaltene precipitation. The cores were measured for gas permeability and porosity once again after removing asphaltene precipitation by washing with toluene and methanol. Finally, the wettability was measured again after re-aging.

Results and Discussion

Minimum Miscibility Pressure

The results of slim-tube tests for the MMP of the system of CO_2-crude oil sample at temperature of 70±0.1°C are shown in Figure 5. The measured oil recovery factors (RFs) versus pore volume (PV) of

injected CO_2 demonstrate that the ultimate oil RFs increased as the operating pressure increased (Figure 5a). This was mainly due to reductions in the interfacial tension and the viscosity of crude oil, attributed to CO_2 dissolution. The ultimate oil RF of each slim-tube test was plotted as a function of injection pressure to determine the MMP, as shown in Figure 5b. The intersection point of the two fitting curves is regarded as the MMP of the CO_2-crude oil system measured by slim-tube test, which is 16.3±0.815 MPa for this crude oil. The conservative error of this conventional experiment is considered less than 5% to measure MMP [48].

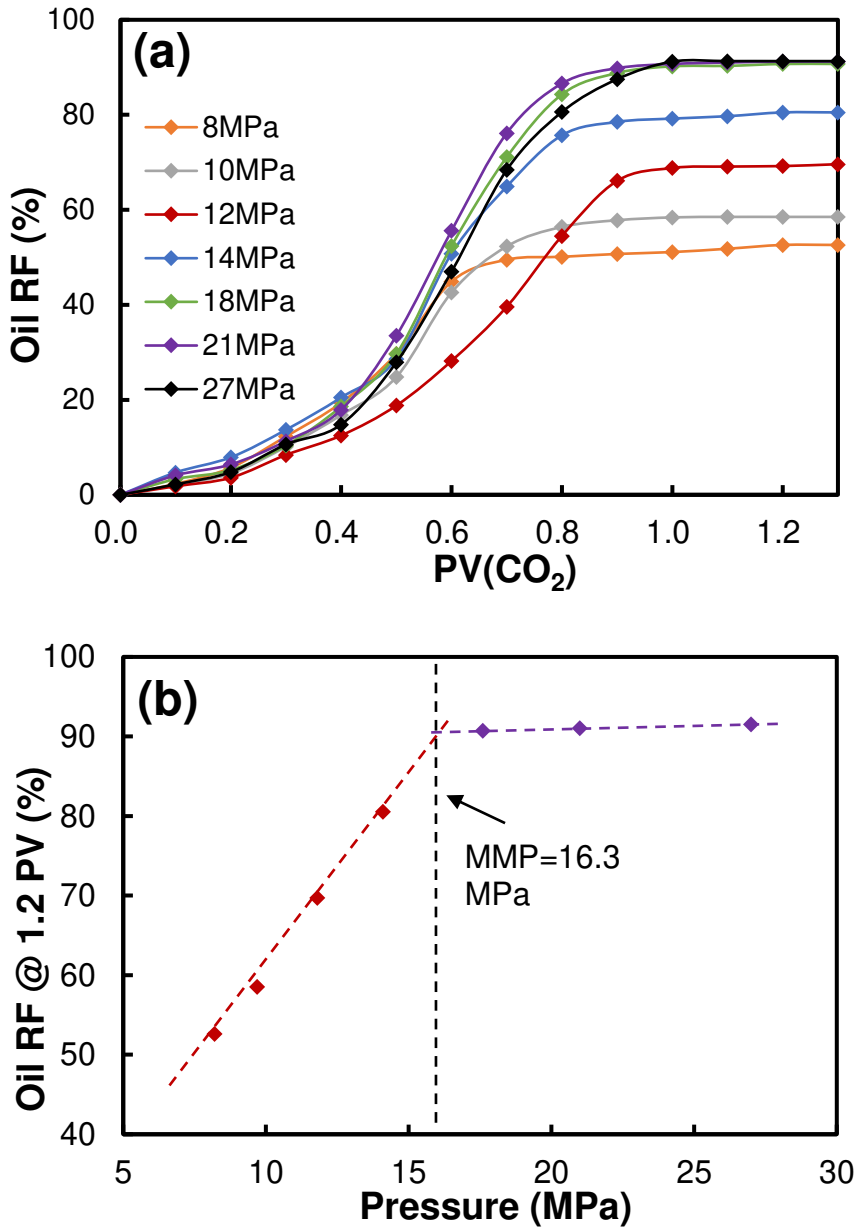

Figure 5. (a) Measured oil RFs as a function of volume of injected CO_2 (in PV) by using the slim-tube apparatus at the operating pressure from 8 MPa to 27 MPa and temperature of 70±0.1°C. (b) Variation of the cumulative oil recovery factor determined at 1.20 pore volumes of CO_2 injected at different operating pressures.

Core pore-throat structure

Five different characteristic patterns of T_2 distribution have been identified in the tight sandstone rocks from the Changqing reservoir [44]. These are (i) a bimodal distribution with a higher left peak and a lower right peak, (ii) a bimodal distribution with a lower left peak but a higher right peak, (iii) a bimodal distribution with similar amplitudes of the two peaks, (iv) a unimodal distribution, and (v) a tri-modal distribution. As for the bimodal distribution, the different or similar amplitudes of the left and right peaks illustrate that the core samples can have rather different or similar fractions of small and large pore-throats. For example, a higher left peak and a lower higher right peak indicates a fraction of greater pore-throats and smaller fraction of larger pore-throats, respectively. Tri-modal distributions imply there may be microcracks present in the core sample (Figure 2). A unimodal distribution indicates that the core sample has a weak heterogeneity with respect to pore-throat sizes. The bimodal distribution was the predominant type of T_2 distribution measured in the 19 cores selected for this study. The limited number of samples used resulted in there being no example of a unimodal distribution available.

The results of CRMI show (Figure 2) that there is no significant difference in the pore distribution of the four cores, but this does not imply that the four cores have the same pore volume. The pore-throats play a dominant role in affecting the permeability of cores, while the pores are the places where the reservoir fluids are stored [49]. The pore-throat distributions of H2 and H3 each have a well-defined peak with a modal value greater than 1 μm. By comparison, H1 and H4 also exhibit a single, but much wider, peak with a modal value less than 1 μm. This implies that H1 and H4 have a higher proportion of large pore-throats, which, if well-connected would provide a high permeability. Since all four core types have been chosen to have practically the same permeability, it is possible to infer that the pores of H1 and H4 are less well-connected for fluid flow even though their individual pore-throats are large. Conversely H2 and H3 have small pore-throats in general and almost none over 2 mm. Since their permeability is the same as that of H1 and H4, it may be inferred that, though connected by small pore-throats the overall connectivity of the pore microstructure is good and pervasive. In addition, the distributions of pore-throat ratio also imply that H1 and H4 have strong heterogeneity in pore-throat microstructure, and H3 has the best pore-throat microstructure.

In CRMI, the intrusion curves for total intrusion, pore body and pore-throat intrusion were recorded simultaneously (Figure 6). According to the distinct mercury intrusion features, the 4 samples can be classified into two types. For samples H1 and H4, the total intrusion is consistent with pore-throat intrusion controlling the increase of pressure. Furthermore, with the increase of pressure, the throat intrusion increases continuously, while the incremental pore body intrusion only occurs over a narrow pressure range, indicating that pore bodies are mainly connected by a small number of relatively large

throats. The very narrow pressure range over which intrusion takes place in H4 is an indicator that this sample may contain microcracks. Samples H2 and H3 belong to the other type, where the total intrusion is controlled by intrusion of the pores, and where the saturation of mercury in both pores and pore-throats increases relatively steadily with increases in pressure. This observation is also an indicator that the pore-throat structure of H2 and H3 is more homogeneous.

The relationship between the logarithm of the capillary pressure and the logarithm of the saturation of the wetting phase is shown in Figure 7. All samples exhibit good linear fits (coefficient of determination, $R^2 > 0.9$). Since the linear fit is carried out in log-log space, the overall relationship between capillary pressure and the saturation of the wetting phase is a power law, which is one of the indicators of fractal behaviour. Consequently, these sandstone samples are generally fractal and can be characterized by using the theories of fractal geometry [50]. The curves of log (S_w) versus log (P_c) breaks into two segments, small pores or throats (corresponding to high capillary pressure) tend to have slopes ranging from -0.25 to -0.41, while large pores were more likely to have slopes close to 0. The fractal dimensions were calculated using the slope of straight part of each curve. The fractal dimensions of small pores or throats can be ranked in increasing order: H3 (2.596) <H2 (2.622) <H1 (2.706) <H4 (2.748), and these values are also given in Table 4. However, the fractal dimensions of large pores are less than 3 but very close to 3, this may mean that large pores cannot be effectively evaluated by this fractal analysis method, while fractal dimension is mainly associated with small pores or throats [51]. In addition, according to Figure 2, the difference in the distribution of the large pores of the four cores is not obvious. The pore-throat structures of samples are evaluated through fractal dimension of small pores or throats, and the results indicate that the pore-throat structures of H2 and H3 are less heterogeneous than those of H1 and H4.

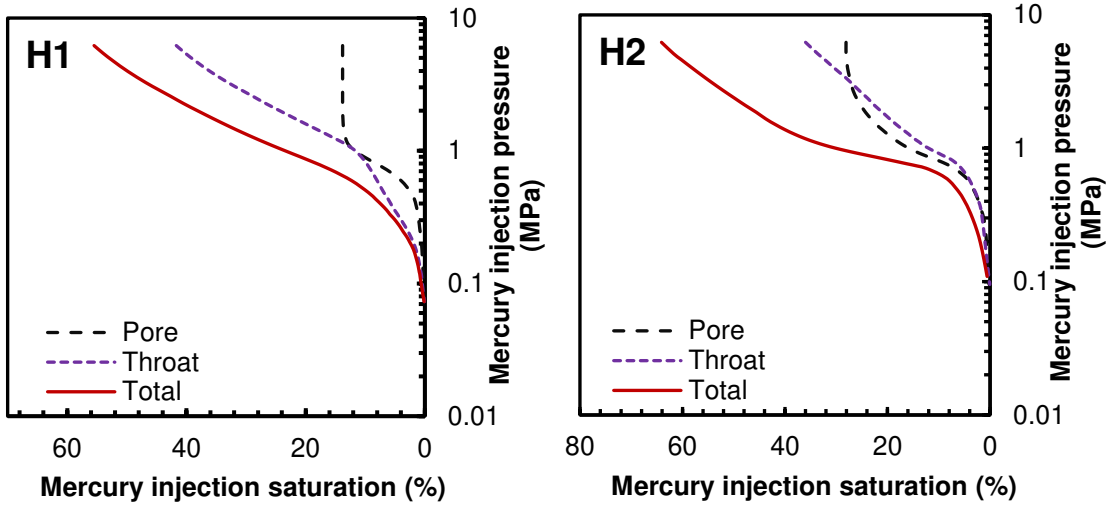

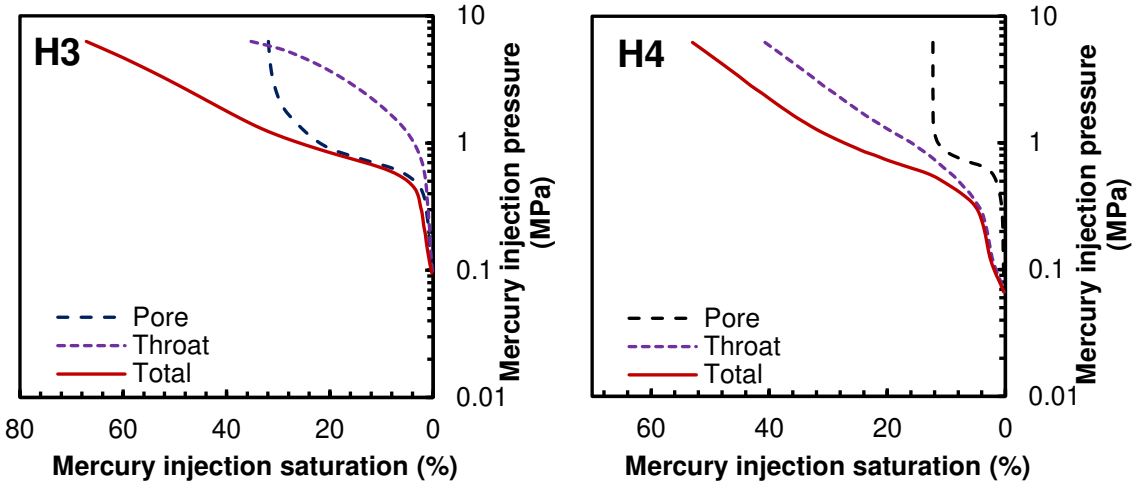

Figure 6. MICP results before core-flooding experiments, showing intrusion into pores, pore-throats and in total.

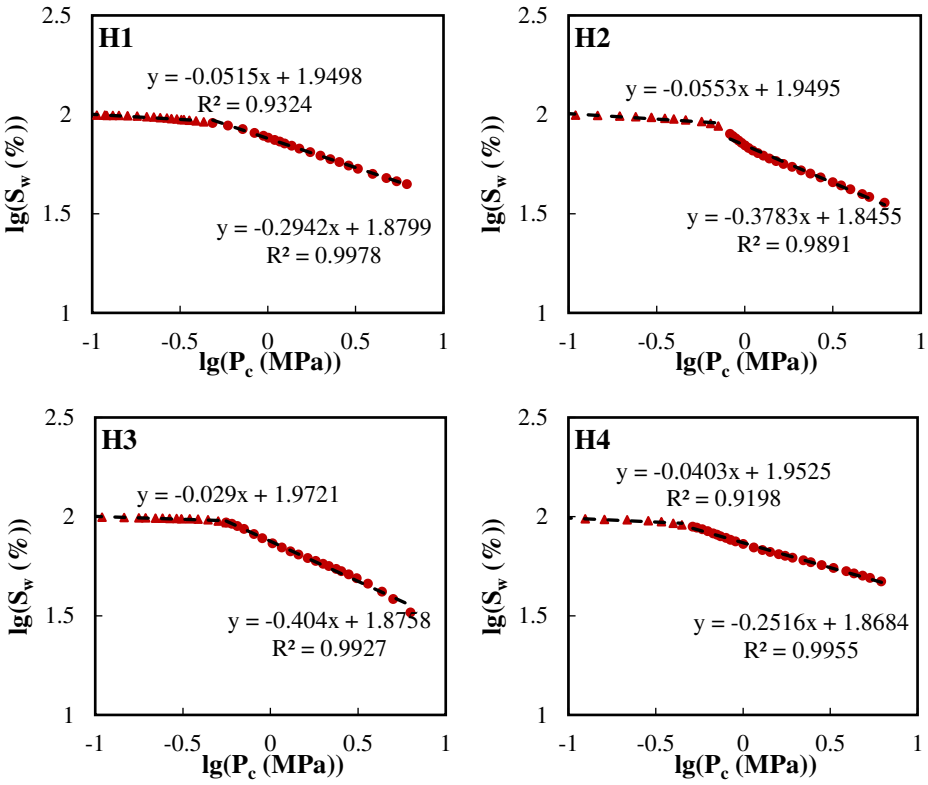

Figure 7. The relationship between capillary pressure and wetting phase saturation of four core samples.

Oil RFs and Residual Oil Distribution

The T_2 spectra given in Figure 8 show the distribution of initial oil before flooding and the residual oil after flooding for each core type. The oil saturation in different sizes of pores increases with radius

when the cores are saturated with oil and are allowed to stand to reach equilibrium. The oil RFs in different sizes of pores also increase with radius after flooding. However, for the cores with different pore size distributions and pore-throat structures, the difference in oil saturation between different sizes of pores is not significant before flooding, but there is a large difference in oil RFs in different sizes of pores after flooding. The heterogeneous pore-throats structures of H1 and H4 lead to much lower oil RFs in the pore sizes related to the 0.1-10 ms T_2 range than that of H2 and H3. In addition, the larger pores of all four cores exhibit only a little difference in oil RFs despite these cores having very different pore-throat structures. In the large pores of H1 and H4, the oil RFs are still high, because these large pores are controlled by a few large throats, and the oil is easier to drive out, which indicates that the oil displacement effect of CO_2 in the largest pores is less affected by the pore structure.

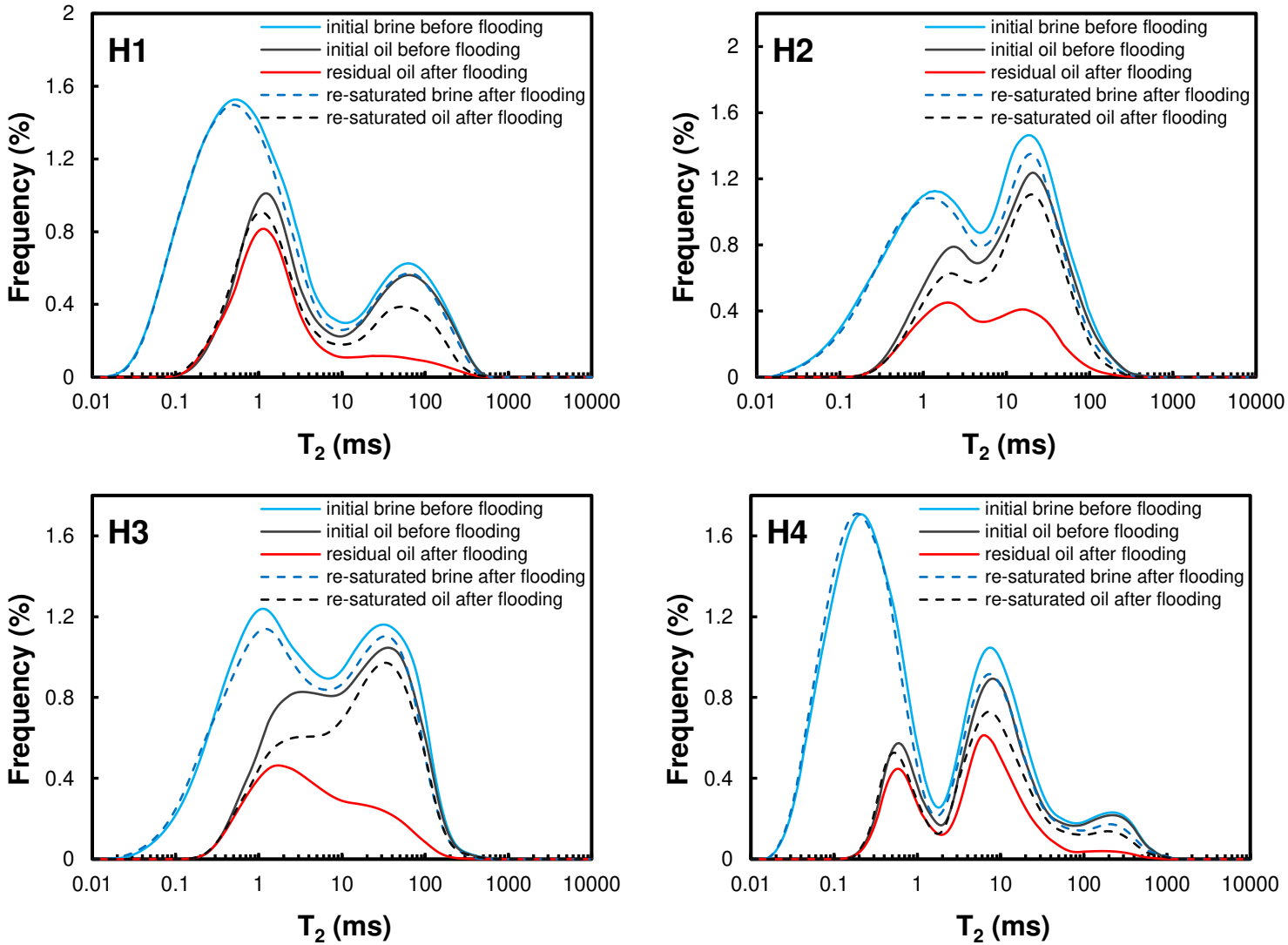

Figure 8. NMR T_2 spectra of initial brine oil distribution in cores before flooding, residual oil and oil re-saturated brine and oil after flooding for each sample.

Figure 9 shows the oil RFs classified against T_2 ranges, which represent pore size ranges. The residual oil in H1 and H4 is mainly distributed in the small pores (<10 ms), represented by the left side of the T_2 spectrum, while a relatively small proportion of residual oil exists in the large pores (>10 ms), and the residual oil distributions in H2 and H3 are more uniform. The overall oil RFs of H2 and H3 are also higher than those of H1 and H4 (Table 6). Furthermore, the overall oil RFs of cores have a good apparently linear relationship with the fractal dimension (Figure 10). Consequently, it may be said that the cores with homogeneous pore-throat structure (H2 an H3) exhibit a more effective oil displacement by CO_2 on the basis of oil recovery and residual oil distribution.

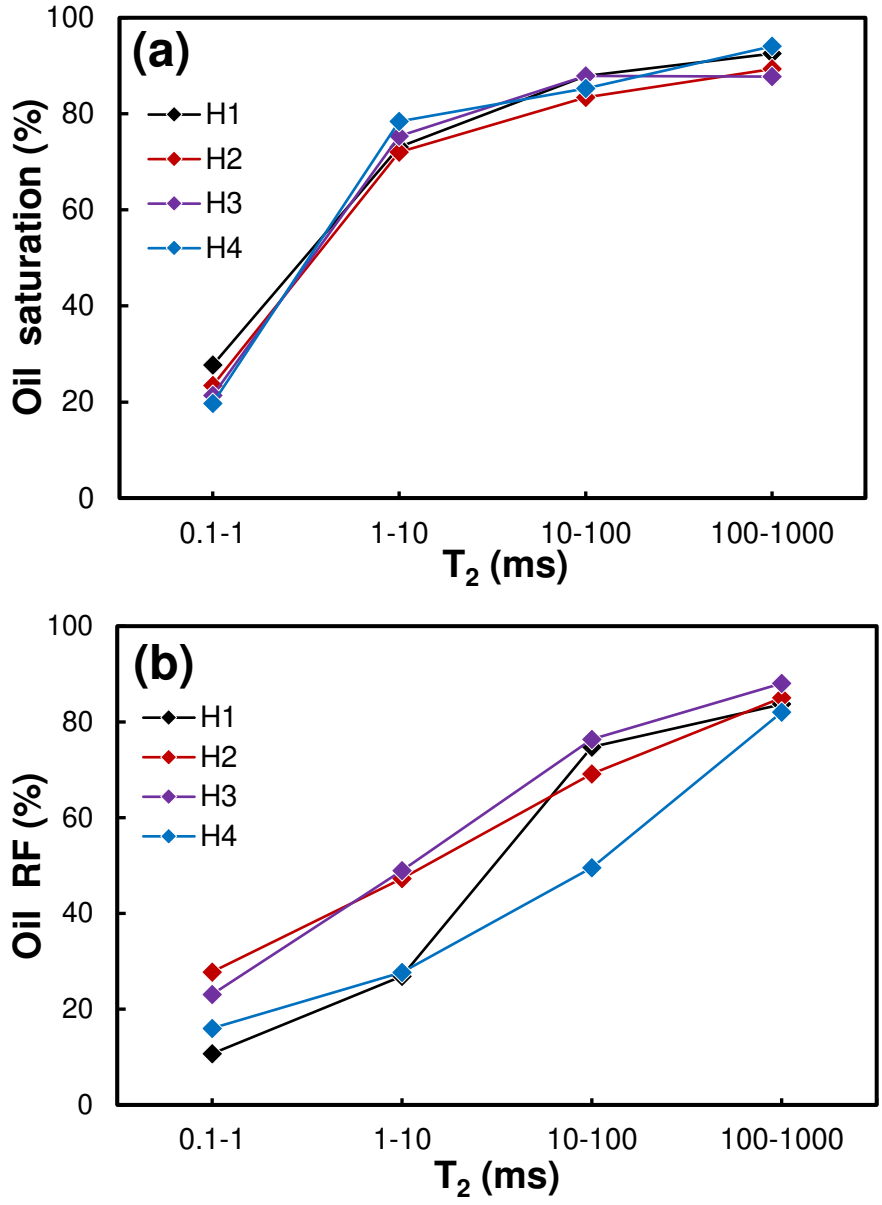

Figure 9. (a) Oil saturation and (b) RF in pores, both as a function of T_2 relaxation time, indicating pores of different sizes.

Table 6. Oil and water saturation before flooding and oil RFs and residual oil after flooding according to NMR T_2 spectra.

Core number	Fractal dimensions	Pore volume (cm^3)	S_{oi} (%)	S_{wc} (%)	Oil RF (%)	residual Oil (%)	Asphaltene in produced oil (wt%)
H1	2.706	4.10	51.39	48.61	43.1	56.9	0.71
H2	2.622	3.91	62.87	37.13	57.7	42.3	0.79
H3	2.596	3.78	65.48	34.52	61.9	38.1	0.85
H4	2.748	3.33	42.33	57.67	39.6	60.4	0.66

Note: S_{oi} is the initial oil saturation and S_{wc} is the connate water saturation, asphaltene in original oil 1.32 wt%.

The asphaltene content of the initial oil was the same for all samples at 1.32wt% (Table 6). By contrast, the asphaltene content in the produced oil varies, but is always less than that in the original oil, indicating that asphaltenes are left in all of the cores to some extent. Asphaltene content in the produced oil is affected by the pore size distribution and heterogeneity of the pore-throat structure. The asphaltene content in produced oil also has a good linear relationship with the fractal dimension (Figure 10), indicating that the pore-throat structure is more homogeneous, and there are less asphaltene precipitates left in the pores, which is advantageous for CO_2-EOR.

We noted in our experiments that the oil produced and collected at the outlet for H2 and H3 was higher in asphaltene than for H1 and H4. Samples H1 and H4 clearly contain more preferential flow paths, especially H4, which contains microcracks. The presence of small pores and pore-throats implies greater displacement resistance, while preferential flow paths result in reduced sweep volumes of the injected CO_2, it is difficult for injected CO_2 to enter small pores [2], which both lead to H1 and H4 having lower oil RFs. Furthermore, the injected CO_2 repeatedly displaces the crude oil on the preferential paths with stronger light-hydrocarbons extraction, greatly increasing the probability of asphaltene precipitation, so the average asphaltene content in the produced oil is lower. The oil produced by the preferential paths tends to be lighter, resulting in the residual oil being heavier than the initial oil in place. It is worth noting that the amount of CO_2 injected during each flooding process is equal. For H2 and H3, more flow paths are generated during the CO_2 flooding, leading to the injected CO_2 dispersed amongst more pores and pore-throats to displace more oil with slight light-hydrocarbons extraction on the crude oil, and ultimately resulting in a higher asphaltene average content in the produced oil.

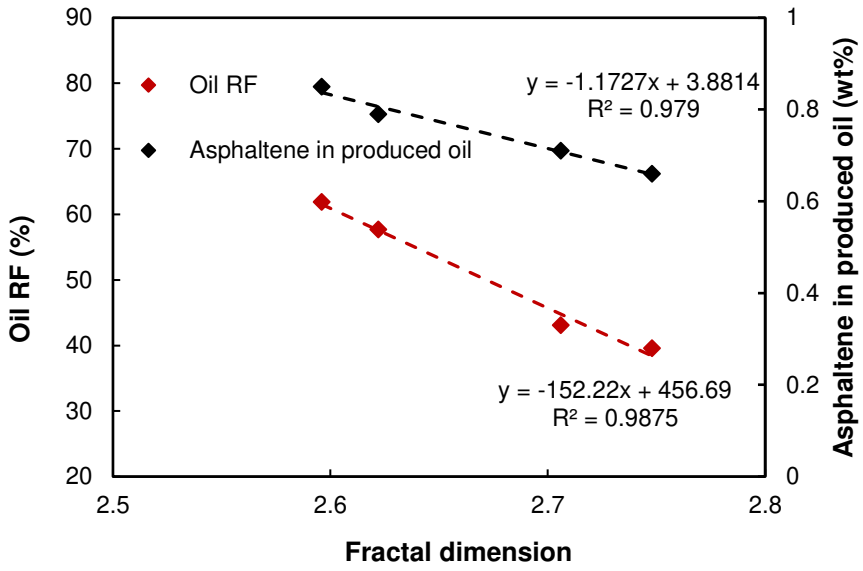

Figure 10. Oil RFs and asphaltene in the produced oil as a function of the fractal dimension of core pore-throat structure.

Porosity and permeability decline

The changes in permeability and porosity of the cores after the flooding experiments are shown in Table 7. The permeability of all cores showed a decline in the range 7-15%, while the porosity decreased by between 1.4% and 2.45%. Calculated uncertainties in individual porosity measurements were less than 3%, and uncertainties in permeability measurements of about 4%, producing uncertainties of less than 6% and about 8% in the calculated declines.

Table 7. Changes in permeability and porosity of cores before and after flooding experiments.

Core number	k_b (mD)	k_a (mD)	k_r (mD)	1-(k_a/k_b) (%)	ϕ_b (%)	ϕ_a (%)	ϕ_r (%)	1-(ϕ_a/ϕ_b) (%)
H1	0.713	0.620	0.721	13.1	14.62	14.38	14.68	1.64
H2	0.742	0.671	0.734	9.6	14.14	13.84	14.25	2.12
H3	0.769	0.711	0.775	7.5	13.62	13.43	13.55	1.40
H4	0.734	0.630	0.722	14.2	11.85	11.56	11.64	2.45

Notes. k_b core permeability before flooding, k_a core permeability after flooding, k_r core permeability after removing asphaltene precipitation, 1-(k_a/k_b) permeability decline, ϕ_b core porosity before flooding, ϕ_a core porosity after flooding, ϕ_r core porosity after removing asphaltene precipitation, 1-(ϕ_a/ϕ_b) porosity decline.

The significant permeability declines are attributed to changes in the microstructure of pores and throats of cores caused by asphaltene precipitation [18]. The asphaltenes begin to precipitate from the crude oil and aggregate to asphaltene particles when CO_2 is injected into cores and the concentration in crude oil reaches a certain value. The migration of asphaltene particles with fluid can cause blockages in the pores and throats of the rocks during flooding [19]. Because permeability is highly

sensitive to the connectedness of the pore-throat structure, blockage or partial blockage at flow pathways can reduce permeability significantly but may have little effect on porosity [49], and the degree of blockage at pore-throats controls the extent of the permeability decrease.

It has been noted that flooding experiments using brine that have been carried out on other cores from the same reservoir show that problems associated with the swelling of clay minerals and inorganic salt scaling caused by high salinity brine have no significant effect on rock porosity and permeability[14]. Additionally, the limited contact area between CO_2, brine and rock and short period of time are not conducive to CO_2–brine–rock interactions [52]. Furthermore and more importantly, the last step in our experiments was to clean the asphaltene precipitation from the cores after flooding. When this was done, it was noted that the restored permeability values were only slightly different from the original ones (± 1.6%). Consequently, we have been able to observe the effect of asphaltene precipitation on both permeability and porosity as a result of flooding with CO_2, as well as our ability to restore the original porosity and permeability when the precipitated asphaltene has been removed. The corollary is that damage to porosity and permeability of cores subsequent to core flooding with CO_2 observed in this paper is mainly due to asphaltene precipitation.

Higher oil RF results from a more efficient sweep of the core by CO_2 (i.e., more of the oil in the core being in contact with CO_2 and being driven out during flooding). One might expect that a more efficient sweep of the core during the flooding process would result in more severe blockage of pores and pore-throats as asphaltene is transported through them, hence producing a larger decrease in permeability. However, greater permeability declines are associated with lower oil RFs in these flooding experiments. The permeability of H1 and H4 with lower oil RFs decreased more significantly than those of H2 and H3 with higher oil RFs. As shown in the left-hand part of Figure 11, the average permeability decline for each 1% change in oil RF of H2 and H3 is each much lower than those for H1 and H4. This may be attributed to the combined effects of a strongly heterogeneous pore-throat microstructure and a smaller average pore-throat size in samples H1 and H4. The permeability decline is consistent with the trend of fractal dimension of core pore-throat structure, and there is a good linear relationship between them, as shown in the right-hand part of Figure 11. This indicates that differences in pore-throat structure of the four cores is the main factor influencing permeability decline, with less permeability damage being associated with larger and more homogeneous pore-throat structures.

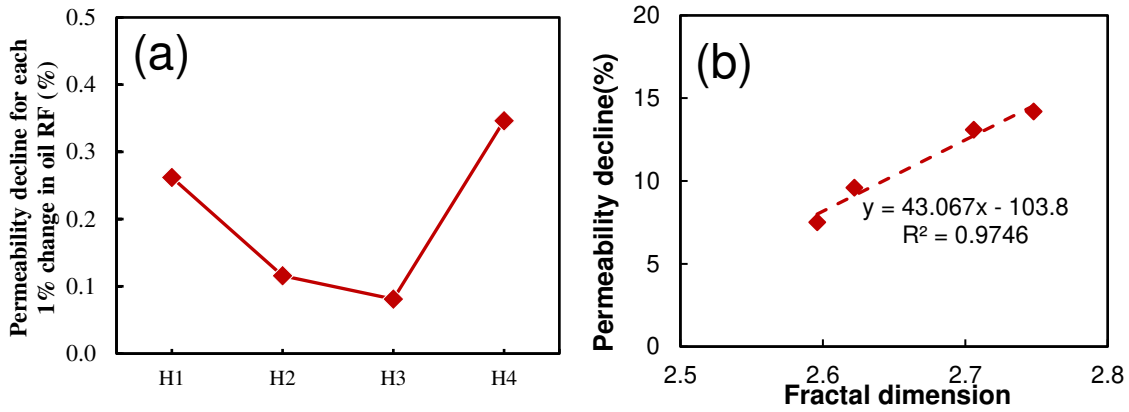

Figure 11. (a) Percentage permeability decline for each 1% change in oil RF for each core sample. (b) Percentage permeability decline as a function of the fractal dimension of the core pore-throat structure.

Figure 12 shows the throat distribution of the four cores as measured by CRMI before and after flooding. There are only slight changes observed in all of the cores, which may be below the experimental uncertainty of the technique. There seems to be a small decrease at large pore-throat sizes, which may indicate that the blockage caused by the migration of asphaltene particles mainly occur at large pore-throats. The variations of distribution frequency of the large throats in H1 and H4 are more significant, in such cores with heterogeneous pore-throat structures, the seepage path composed of a few large pore-throats contributes mostly to the permeability. Consequently, if the main seepage path is preferentially blocked during the flooding process, there is serious damage to the permeability of the reservoir rock, and the changes in permeability of cores with average smaller throat become more sensitive to blockage [21, 53]. The more homogenous pore-throat structures of H2 and H3 have an advantage not only in oil recovery, but also in resisting the decrease in permeability caused by asphaltene precipitation migration.

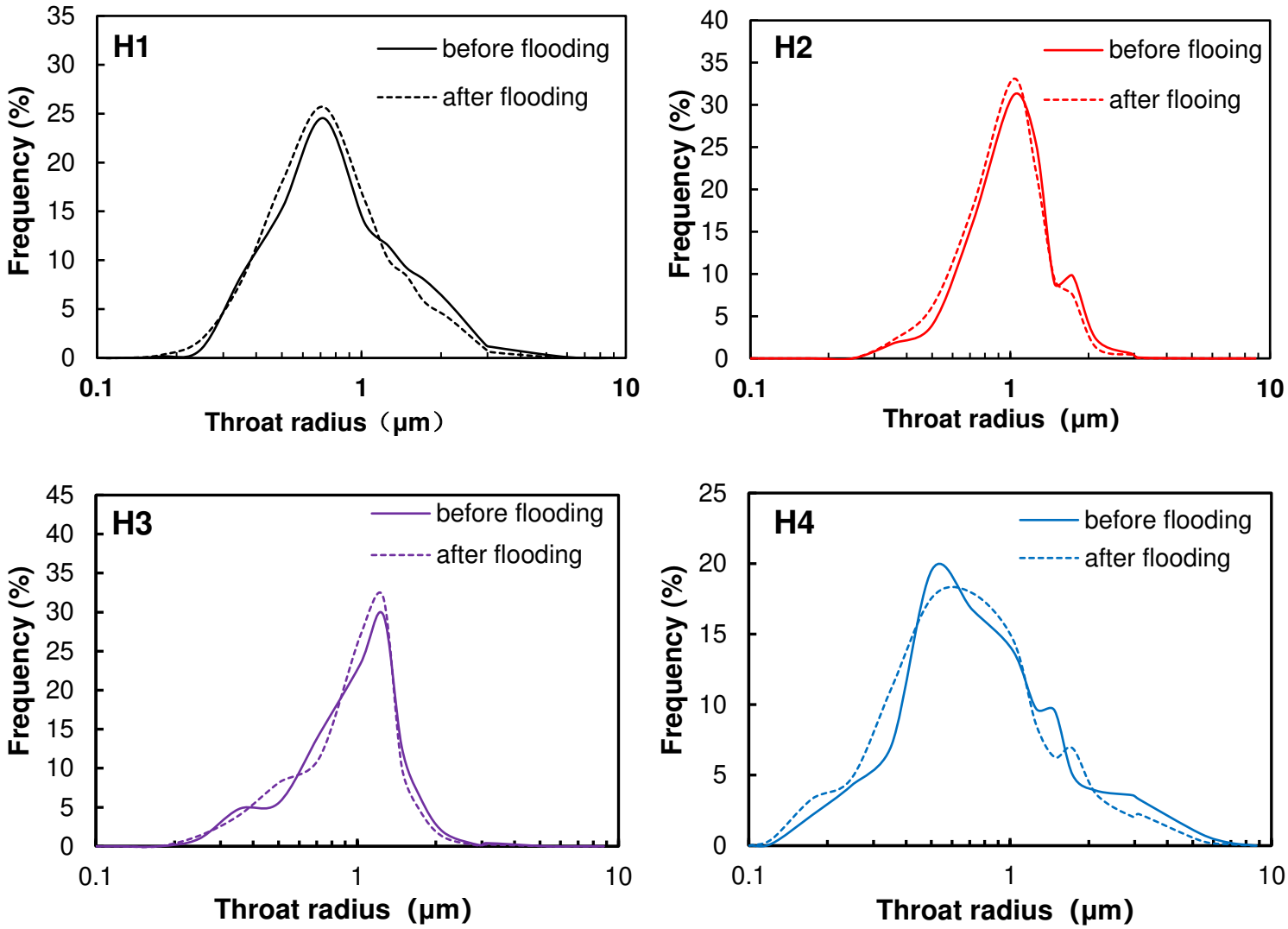

Figure 12. Pore-throats radius distributions for each of the 4, both before and after core-flooding.

Wettability

Changes in wettability of cores are shown in Table 8. The water-wetness of the rock is weakened after flooding, which is attributed to the adsorption of asphaltene precipitation on the pore surface of the rock. The mechanism of wettability alteration by asphaltene deposition is illustrated in Figure 13. The cores were initially water-wet, implying that their internal pore surfaces were covered by a film of water, negatively charged [54-56] and attached by hydrogen bonding. When CO_2 dissolves into the crude oil, the asphaltene molecules begin to aggregate. Due to the high polarity of asphaltene molecules, water films start to destabilize and eventually rupture. The polar ends of the asphaltene are positively charged and adsorbed on the pore surface, exposing the hydrocarbon end and making the surface more oil-wet [57]. In all cores CO_2 core flooding weakened the overall water wettability of the core rather than making the core completely oil-wet, although for H2 the transformation towards oil wetness was considerable. Once the asphaltene precipitation had been removed from the cores by cleaning, the Amott-Harvey indexes returned to values very close to their initial values, showing that the water-wettability of the cores is restored. While it is known that the presence of carbonated water can make the rock more water-wet [58], in our flooding experiments CO_2–brine–rock interaction does not dominate, and the change in the wettability is mainly controlled by asphaltene precipitation.

Table 8. Wettability of cores before and after flooding.

Core number	Water index (I_w)	Oil index (I_o)	Amott-Harvey (I_w-I_o)	
H1	0.912	0.005	0.907	Before flooding
H2	0.755	0.076	0.679	
H3	0.817	0.013	0.804	
H4	0.85	0.045	0.805	
H1	0.686	0.022	0.664	After flooding
H2	0.455	0.182	0.273	
H3	0.536	0.093	0.443	
H4	0.649	0.115	0.534	
H1	0.899	0.012	0.887	After removing asphaltene precipitation and aging again in brine
H2	0.813	0.064	0.749	
H3	0.774	0.028	0.746	
H4	0.819	0.047	0.772	

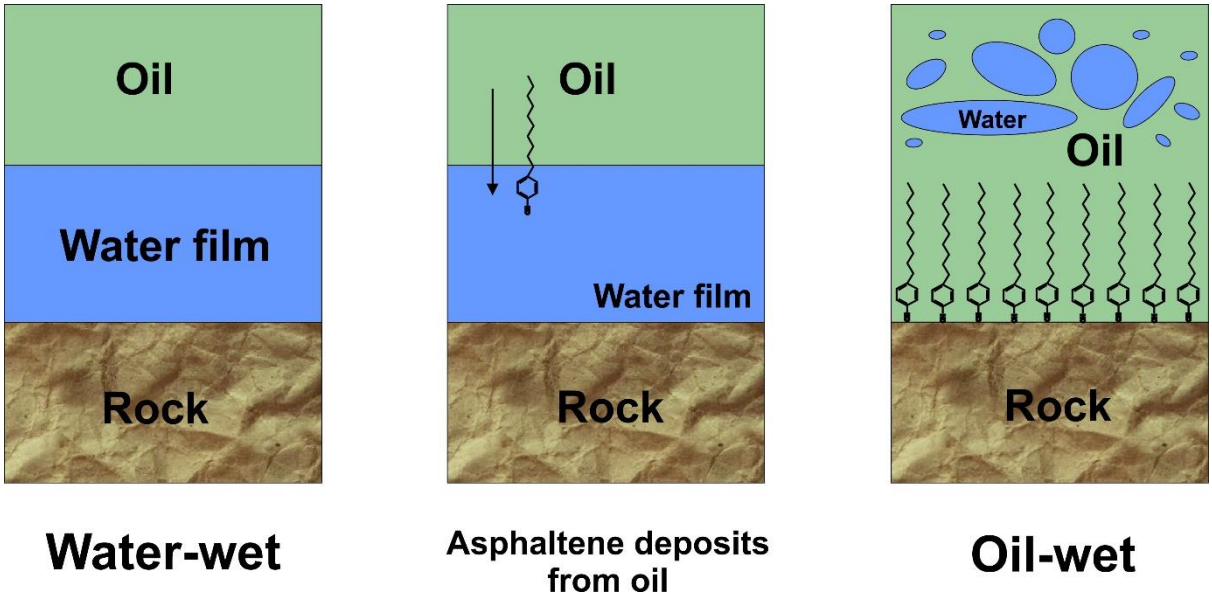

Figure 13. Mechanism of wettability alteration of pore surface by asphaltene precipitation.

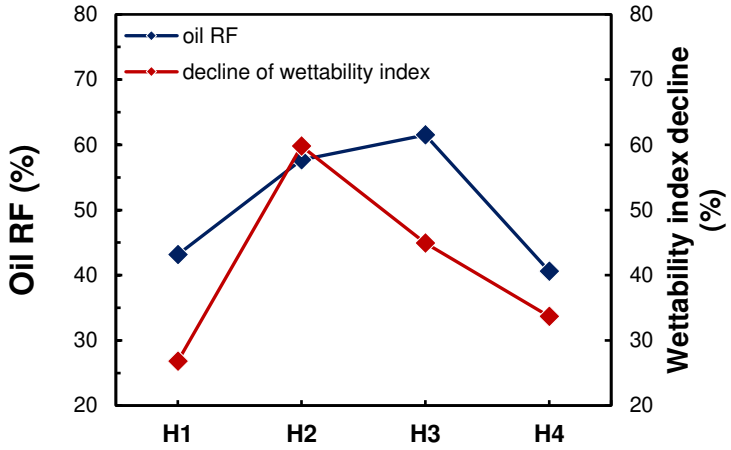

Figure 14. Oil RFs and wettability changes

The wettability of H2 and H3 changes more than that of H1 and H4, which is attributed to the difference in oil RFs caused by the difference in pore-throat structure. The magnitude of the wettability alteration of the four cores has the same trend as oil RFs, as shown in Figure 14. As the homogeneous pore-throat structure of H2 and H3 allows CO_2 to enter more and smaller pores and contact more crude oil [1], more asphaltene precipitates adsorb to more pore surface, resulting in greater changes in overall wettability of cores.

Distribution of Variations in Petrophysical Properties

The T_2 spectra given in Figure 8 show the distribution of initial oil and brine before flooding and re-saturated oil and brine after flooding. The variation in oil saturation (defined as S_{ov}, where $S_{ov}= S_{ob}-S_{oa}$, and S_{ob} is the initial oil saturation before flooding, solid line, and S_{oa} is the oil re-saturation after flooding, dotted line) represents the degree of change in the oil saturation of the cores after flooding. As well as,

the variation in brine saturation (S_{wv}, where S_{wv}= S_{wb}-S_{wa}, and S_{wb} is the brine saturation before flooding, solid line, and S_{wa} is the brine re-saturation after flooding, dotted line) represents the degree of change in the brine saturation of the cores after flooding.

Oil and brine re-saturation after flooding is affected by two factors; (i) blockage of the pore-throats, and (ii) changes to the wettability of cores [14, 19]. When the throats connecting pores are blocked due to the migration of asphaltene precipitation particles with fluid in the rocks, some pores in the rock are not re-saturated with oil or brine completely. Consequently, the signal amplitude of oil and brine in these pores on the T_2 spectrum shows significant decline after re-saturation. S_{wv} and S_{ov} represent the comprehensive changes in rock physical properties after flooding affected by these two factors. The asphaltene precipitate adsorbs to the surface of the pores, making the asphaltene precipitated rocks more oil-wet. This process of progressive oil-wettening aids oil re-saturation. Therefore, S_{ov} is the result of two opposite effects, reflecting the combined results of throat blockage and wettability changes. Generally, the value of S_{ov} is greater than zero, which indicates that the effect of blockage at the throats is greater than that of the change in wettability during oil re-saturation. Unlike S_{ov}, because the oil wettability of the pore walls is enhanced due to the asphaltene precipitation, both of these factors play a role in resisting water re-saturation to increase the value of S_{wv}. Due to the blockage at throats and changes in wettability, the size of the water droplets in the pores of the rock after re-saturated water is reduced, especially in the large pores and associated pore-throats as the main place of CO_2 flooding, consequently the signal amplitude of large pores measured in the T_2 spectrum is reduced, and the signal amplitude of the small pores on the left side of the T_2 spectrum is slightly larger than that before flooding. However, the volume of the re-saturated water in cores in the T_2 spectrum is generally reduced.

The S_{ov} is caused by the crude oil in the pores being displaced by CO_2, high oil RF is likely to result in more blockage of asphaltene particles at throats and large wettability variation under the same displacement pattern. However, Figure 15a shows the opposite result, the oil RFs of H2 and H3 are higher than those of H1 and H4, but H2 and H3 have smaller S_{ov} values. Figure 15b indicates that the result may be attributed to the difference in pore-throat structure between H2, H3 and H1, H4. On the one hand, although more oil production means more asphaltene precipitation in H2 and H3 during the flooding process, these asphaltene precipitates did not form severe blockage as in H1 and H4, causing serious damage to the pore-throats structure of rocks, which implies that the type of pore-throat microstructure of H2 and H3, especially H3, is more resistant to damage to rock properties by the migration of asphaltene precipitation. Moreover, more asphaltene precipitation also implies that H2 and H3 undergo large changes in wettability, which aids oil re-saturation. Consequently, S_{ov} decreases with increasing oil RF and increases with increasing fractal dimension.

Figure 15 indicates that S_{ov} and S_{wv} of the four cores show opposite trends, H1 and H4 have large S_{ov} values, but the values of S_{wv} are smaller than those of H2 and H3. The pore space occupied and throats

blocked by asphaltene deposition are constant during brine and oil re-saturation after flooding, so that the S_{ov} and S_{wv} of four cores should share similar trends in the case of eliminating the factor of wettability changes, theoretically [14]. This is attributed to the fact that changes in wettability increase S_{wv} but decrease S_{ov}. Since both S_{ov} and S_{wv} contain a factor that causes blockage at pores and throats in rocks, the value of S_{wv}-S_{ov} partially eliminates this factor, representing the trend of changes in wettability, just like the calculation and expression of the Amott-Harvey index. As expected, the changes in wettability of the four cores obtained by S_{ov}-S_{wv} is consistent with the results of the measured Amott-Harvey index (Figure 16).

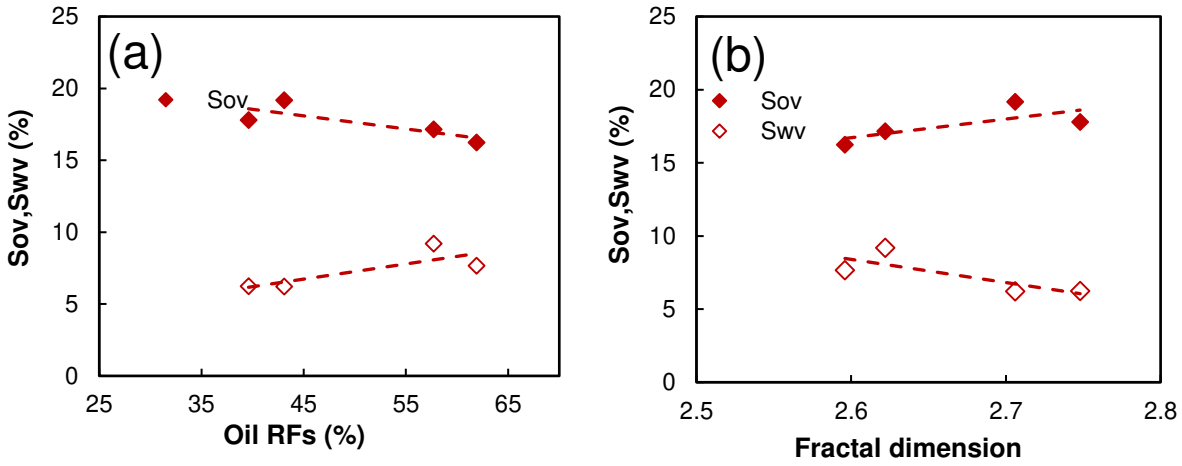

Figure 15. S_{ov} and S_{wv} as function of (a) oil recovery factor, and (b) fractal dimension.

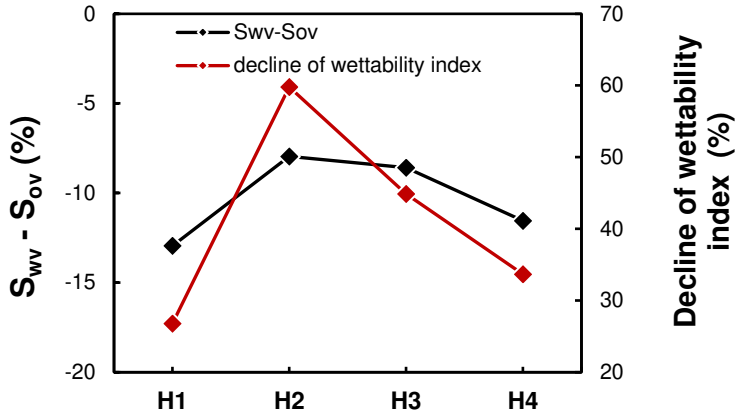

Figure 16. S_{wv}-$S_{ov}$and percentage decline the Amott-Harvey wettability index for each of the four cores studied in this work.

Figure 17 shows the oil RF and S_{ov} as a function of the T_2 value from NMR, representing differences in pore size. The values of S_{ov} of pores with different sizes in H1 and H4 increase with the oil RFs. The smaller S_{ov} in the small pores of H1 and H4 is caused by little oil production. Small pores and associated pore-throats are difficult to sweep of oil during flooding, resulting in less asphaltene precipitation and small S_{ov} values. The large RF in the large pores indicates that these large pores are the main producers of oil, and by implication they are also the main pathways of fluid flow. Such pathways are also the main locations where asphaltene precipitation, migration and adsorption occur. The structure of these pores and associated pore-throats is more likely to be modified by asphaltene precipitation, resulting in large S_{ov} values. However, the values of S_{ov} do not increase strictly with the increase of oil RFs in H2 and H3, especially in H3. Although the pore-throats are partially blocked and the permeability is reduced, it seems that the oil re-saturation of the larger pores is not greatly affected, and the difference in S_{ov} in pores of different sizes is relatively small. Blockage at pore-throats and wettability changes evenly across pores of all sizes, indicating that a homogeneous pore-throat structure is advantageous for the large pores and associated pore-throats to resist the changes in the pore-throat structure caused by asphaltene precipitation and migration.

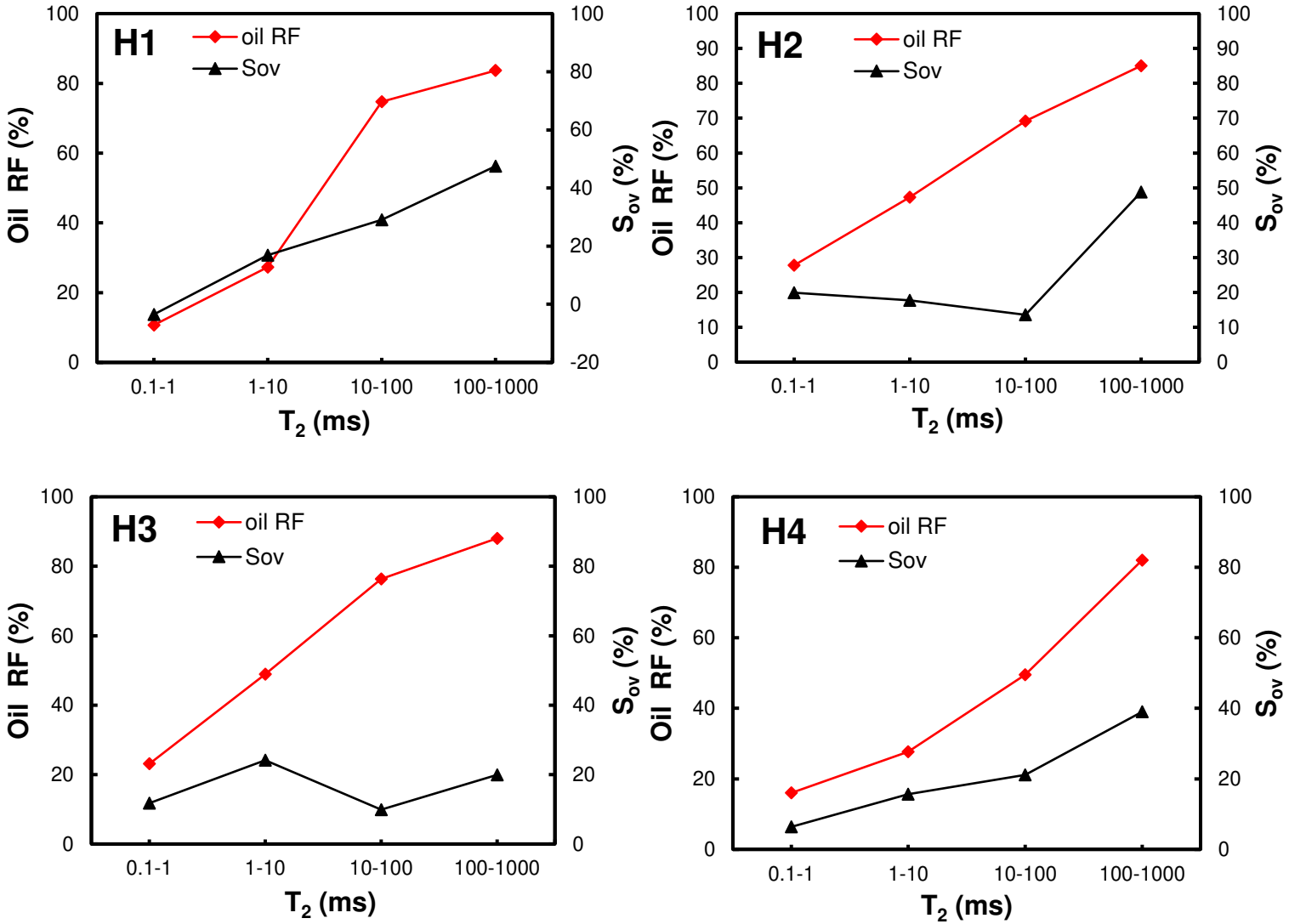

Figure 17. Oil RF and S_{ov} as a function of T_2 relaxation time for each of the different core samples.

Conclusions

In this paper, four core samples with very similar permeabilities but different pore size distributions and pore-throat structures were flooded by CO_2 under miscible conditions at reservoir temperature and pressure. The oil production and residual oil distribution of each core were evaluated, and the blockage of pore-throats, permeability decline and wettability variation were compared. Based on the experimental results, the following conclusions can be drawn.

The total oil recovery factors of cores with heterogeneous pore-throats structures are 14-23% lower than those of homogeneous cores with a larger pore-throats.The produced oil from the cores with smaller and more heterogeneous pore-throat structures are slightly lower in asphaltene content, indicating that more asphaltene remains in the cores.

The permeability of the two heterogeneous core decreased by 13.1% and 14.2% after CO_2 flooding, which we attribute to the blockage of pores and pore-throats caused by the migration of asphaltene particles. By contrast, while the permeability decline of the two cores with larger and more homogeneous pore-throat microstructures was 7.5% and 9.6%, i.e., about 4-7% smaller.

The Amott-Harvey indexes of cores decrease by 25-60%, with the cores with larger and more homogeneous pore-throat microstructure becoming less water-wet due to greater degrees of asphaltene precipitation adsorbed onto a greater pore surface area within the rock. We hypothesize that this effect is ultimately caused by the larger sweep volume of injected CO_2 for the cores with the more homogeneous pore-throat size distributions.

The values of S_{ov} and S_{wv} represent the degree of comprehensive changes in petrophysical properties of cores after flooding. Cores with larger and more homogeneous pore-throat microstructures have a more homogeneous distribution of petrophysical properties, while heterogeneous cores exhibit a much wider distribution of petrophysical properties.

Overall, it is possible to say that cores with larger pores and pore-throats, and which exhibit more homogeneous pore-throat size distributions are more resistant to damage to permeability caused by asphaltene precipitation while generating high oil RFs, but are susceptible to becoming more weakly water-wet. Consequently, rocks with large pores and pore-throats and with homogeneous pore-throat distributions will undergo less asphaltene precipitation and are therefore more favorable for miscible CO_2 flooding as an EOR intervention.

Acknowledgments

Thanks are given to the China Scholarship Council for funding the opportunity of the lead author to research at The University of Leeds, UK. This research is supported by National Natural Science Foundation of China, “Study on the physical basis of seepage in extra-deep clastic reservoirs”

(51774300), and "Key technologies for CO_2 flooding and storage" of the 13th Five-Year National Major Science and Technology Project (2016ZX05016006-004).

References

(1) Wang, R., Chi, Y., Zhang, L., He, R., Tang, Z. and Liu, Z., 2018. Comparative studies of microscopic pore-throat characteristics of unconventional super-low permeability sandstone reservoirs: Examples of Chang 6 and Chang 8 reservoirs of Yanchang Formation in Ordos Basin, China. *Journal of Petroleum Science and Engineering*, *160*, pp. 72-90.

(2) Jia, B., Tsau, J.S. and Barati, R., 2018. Role of molecular diffusion in heterogeneous, naturally fractured shale reservoirs during CO2 huff-n-puff. *Journal of Petroleum Science and Engineering*, 164, pp.31-42.

(3) Li, P., Zheng, M., Bi, H., Wu, S. and Wang, X., 2017. Pore-throat structure and fractal characteristics of tight oil sandstone: a case study in the Ordos Basin, China. *Journal of Petroleum Science and Engineering*, 149, pp. 665-674.

(4) Ampomah, W., Balch, R., Cather, M., Rose-Coss, D., Dai, Z., Heath, J., Dewers, T. and Mozley, P., 2016. Evaluation of CO_2 storage mechanisms in CO_2 enhanced oil recovery sites: Application to Morrow sandstone reservoir. *Energy & Fuels*, 30(10), 8545-8555.

(5) Jia, B., Tsau, J.S. and Barati, R., 2019. A review of the current progress of CO_2 injection EOR and carbon storage in shale oil reservoirs. *Fuel*, 236, pp.404-427.

(6) Or, C., Sasaki, K., Sugai, Y., Nakano, M. & Imai, M., 2016. Swelling and viscosity reduction of heavy oil by CO_2-gas foaming in immiscible condition. *SPE Reservoir Evaluation & Engineering*, *19*(02), 294-304.

(7) Abedini, A., Farshid, T., 2014. On the CO_2 storage potential of cyclic CO_2 injection process for enhanced oil recovery. *Fuel*, 124, 14-27.

(8) Jia, B., Jyun-Syung, T., Reza, B., 2019. A review of the current progress of CO_2 injection EOR and carbon storage in shale oil reservoirs. *Fuel*, 236, 404-427.

(9) Cao, M. and Gu, Y., 2013. Oil recovery mechanisms and asphaltene precipitation phenomenon in immiscible and miscible CO_2 flooding processes. *Fuel*, *109*, pp. 157-166.

(10) Wang, Q., Lorinczi, P. and Glover, P.W., 2020. Oil production and reservoir damage during miscible CO_2 injection. *The Leading Edge*, 39(1), pp.22-28.

(11) Cao, M. and Gu, Y., 2012. Physicochemical characterization of produced oils and gases in immiscible and miscible CO_2 flooding processes. *Energy & Fuels*, *27*(1), pp. 440-453.

(12) Ghorbani, M., Momeni, A., Safavi, S. and Gandomkar, A., 2014. Modified vanishing interfacial tension (VIT) test for CO_2–oil minimum miscibility pressure (MMP) measurement. *Journal of Natural Gas Science and Engineering*, 20, 92-98.

(13) Hawthorne, S. B., Miller, D. J., Jin, L., & Gorecki, C. D., 2016. Rapid and simple capillary-rise/vanishing interfacial tension method to determine crude oil minimum miscibility pressure: pure and mixed CO_2, methane, and ethane. *Energy & Fuels*, 30(8), 6365-6372.

(14) Qian, K., Yang, S., Dou, H.E., Pang, J. and Huang, Y., 2019. Formation damage due to asphaltene precipitation during CO_2 flooding processes with NMR technique. *Oil & Gas Science and Technology–Revue d'IFP Energies nouvelles*, *74*, p.11.

(15) Srivastava, R.K., Huang, S.S. and Dong, M., 1999. Asphaltene deposition during CO_2 flooding. *SPE production & facilities*, *14*(04), pp. 235-245.

(16) Hamouda, A. A., Chukwudeme, E. A., & Mirza, D., 2009. Investigating the effect of CO_2 flooding on asphaltenic oil recovery and reservoir wettability. *Energy & Fuels*, *23*(2), 1118-1127.

(17) Wang, Q., Yang, S., Lorinczi, P., Glover, P.W. and Lei, H., 2020. Experimental Investigation of Oil Recovery Performance and Permeability Damage in Multilayer Reservoirs after CO_2 and Water–Alternating-CO_2 (CO_2–WAG) Flooding at Miscible Pressures. *Energy & Fuels*. 34, 1, 624-636

(18) Jafari Behbahani, T., Ghotbi, C., Taghikhani, V., & Shahrabadi, A., 2012. Investigation on asphaltene deposition mechanisms during CO_2 flooding processes in porous media: a novel experimental study and a modified model based on multilayer theory for asphaltene adsorption. *Energy & Fuels*, *26*(8), 5080-5091.

(19) Okwen, R.T., 2006. Formation Damage by CO_2 Asphaltene Precipitation. In *SPE International Symposium and Exhibition on Formation damage control*. Society of Petroleum Engineers.

(20) Uetani T., 2014. Wettability alteration by asphaltene deposition: A field example[C]//Abu Dhabi International Petroleum Exhibition and Conference. Society of Petroleum Engineers.

(21) Lai, J., & Wang, G., 2015. Fractal analysis of tight gas sandstones using high-pressure mercury intrusion techniques. *Journal of Natural Gas Science and Engineering*, *24*, 185-196.

(22) Hu, Q., Ewing, R. P., & Dultz, S., 2012. Low pore connectivity in natural rock. *Journal of contaminant hydrology*, *133*, 76-83.

(23) Wang, H., Liu, Y., Song, Y., Zhao, Y., Zhao, J., & Wang, D., 2012. Fractal analysis and its impact factors on pore structure of artificial cores based on the images obtained using magnetic resonance imaging. *Journal of Applied Geophysics*, *86*, 70-81.

(24) Al-Zainaldin, S., Glover, P.W.J. and Lorinczi, P., 2017. Synthetic Fractal Modelling of Heterogeneous and Anisotropic Reservoirs for Use in Simulation Studies: Implications on Their Hydrocarbon Recovery Prediction. Transport in Porous Media, 116(1), pp. 181-212.

(25) Glover, P.W.J., Lorinczi, P., Al-Zainaldin, S., Al-Ramadan, H., Daniel, G. and Sinan, S., 2018. Advanced fractal modelling of heterogeneous and anisotropic reservoirs, SPWLA 59th Annual Logging Symposium 2018.

(26) Glover, P.W.J., Lorinczi, P., Al-Zainaldin, S., Al-Ramadhan, H., Sinan, S. and Daniel, G., 2019. A fractal approach to the modelling and simulation of heterogeneous and anisotropic reservoirs, Society of Petroleum Engineers - SPE Offshore Europe Conference and Exhibition 2019, OE.

(27) Bikkina, P., Wan, J., Kim, Y., Kneafsey, T.J. and Tokunaga, T.K., 2016. Influence of wettability and permeability heterogeneity on miscible CO_2 flooding efficiency. *Fuel*, 166, 219-226.

(28) Chatzis, I., Morrow, N.R. and Lim, H.T., 1983. Magnitude and detailed structure of residual oil saturation. *Society of Petroleum Engineers Journal*, *23*(02), pp. 311-326.

(29) Lengler, U., De Lucia, M., & Kühn, M., 2010. The impact of heterogeneity on the distribution of CO_2: Numerical simulation of CO_2 storage at Ketzin. *International Journal of Greenhouse Gas Control*, *4*(6), 1016-1025.

(30) Mendoza de la Cruz, J. L., Argüelles-Vivas, F. J., Matías-Pérez, V., Durán-Valencia, C. D. L. A., & López-Ramírez, S., 2009. Asphaltene-induced precipitation and deposition during pressure depletion on a porous medium: an experimental investigation and modeling approach. *Energy & Fuels*, *23*(11), 5611-5625.

(31) Ali, M.A., 2012. Laboratory Investigation of Dynamic Growth of Asphaltene Deposition and Formation Damage on Sandstone Cores. In *SPE Kuwait International Petroleum Conference and Exhibition*. Society of Petroleum Engineers.

(32) Wang, C., Li, T., Gao, H., Zhao, J., & Li, H. A., 2017. Effect of asphaltene precipitation on CO_2-flooding performance in low-permeability sandstones: a nuclear magnetic resonance study. *RSC Advances*, *7*(61), 38367-38376.

(33) Zanganeh, P., Ayatollahi, S., Alamdari, A., Zolghadr, A., Dashti, H. and Kord, S., 2012. Asphaltene deposition during CO_2 injection and pressure depletion: a visual study. *Energy & Fuels*, *26*(2), pp. 1412-1419.

(34) Kord, S., Mohammadzadeh, O., Miri, R. and Soulgani, B.S., 2014. Further investigation into the mechanisms of asphaltene deposition and permeability impairment in porous media using a modified analytical model. *Fuel*, *117*, pp. 259-268.

(35) Sim, S.S.K., Okatsu, K., Takabayashi, K. and Fisher, D.B., 2005. Asphaltene-induced formation damage: effect of asphaltene particle size and core permeability. In SPE Annual Technical Conference and Exhibition. Society of Petroleum Engineers.

(36) Fakher, S. and Imqam, A., 2018. Investigating and Mitigating Asphaltene Precipitation and Deposition in Low Permeability Oil Reservoirs during Carbon Dioxide Flooding to Increase Oil Recovery. In *SPE Annual Caspian Technical Conference and Exhibition*. Society of Petroleum Engineers.

(37) Papadimitriou, N.I., Romanos, G.E., Charalambopoulou, G.C., Kainourgiakis, M.E., Katsaros, F.K. and Stubos, A.K., 2007. Experimental investigation of asphaltene deposition mechanism during oil flow in core samples. *Journal of Petroleum Science and Engineering*, *57*(3-4), pp. 281-293.

(38) Hosseini, E., 2019. Experimental investigation of effect of asphaltene deposition on oil relative permeability, rock wettability alteration, and recovery in WAG process. *Petroleum Science and Technology*, *37*(20), pp. 2150-2159.

(39) Zendehboudi, S., Ahmadi, M. A., Mohammadzadeh, O., Bahadori, A., & Chatzis, I. (2013). Thermodynamic investigation of asphaltene precipitation during primary oil production: laboratory and smart technique. *Industrial & Engineering Chemistry Research*, *52*(17), 6009-6031.

(40) Wang, C., Li, T., Gao, H., Zhao, J. and Gao, Y., 2018. Quantitative study on the blockage degree of pores due to asphaltene precipitation in low-permeability reservoirs with NMR technique. *Journal of Petroleum Science and Engineering*, *163*, pp. 703-711.

(41) Kord, S., Miri, R., Ayatollahi, S. and Escrochi, M., 2012. Asphaltene deposition in carbonate rocks: experimental investigation and numerical simulation. *Energy & Fuels*, 26(10), pp.6186-6199.

(42) Wang, Z., Yang, S., Lei, H., Yang, M., Li, L. and Yang, S., 2017. Oil recovery performance and permeability reduction mechanisms in miscible CO_2 water-alternative-gas (WAG) injection after continuous CO_2 injection: An experimental investigation and modelling approach. *Journal of Petroleum Science and Engineering*, 150, 376-385.

(43) Zhao, X., Yang, Z., Lin, W., Xiong, S. and Wei, Y., 2018. Characteristics of microscopic pore-throat structure of tight oil reservoirs in Sichuan Basin measured by rate-controlled mercury injection. *Open Physics*, *16*(1), pp. 675-684.

(44) Lei, H., Yang, S., Qian, K., Chen, Y., Li, Y. and Ma, Q., 2015. Experimental investigation and application of the asphaltene precipitation envelope. *Energy & Fuels*, *29*(11), pp. 6920-6927.

(45) Gao, H. and Li, H., 2015. Determination of movable fluid percentage and movable fluid porosity in extra-low permeability sandstone using nuclear magnetic resonance (NMR) technique. *Journal of Petroleum Science and Engineering*, *133*, pp. 258-267.

(46) Yuan, H. H., & Swanson, B. F., 1989. Resolving pore-space characteristics by rate-controlled porosimetry. *SPE Formation Evaluation*, *4*(01), 17-24.

(47) Tiab, D. and Donaldson, E.C., 2016. Porosity and permeability. Petrophysics. Theory and Practice of Measuring Reservoir Rock and Fluid Transport Properties. 4th ed. *Elsevier, Amsterdam*, pp.67-186.

(48) Li, H., Qin, J., & Yang, D., 2012. An improved CO_2–oil minimum miscibility pressure correlation for live and dead crude oils. *Industrial & Engineering Chemistry Research*, *51*(8), 3516-3523.

(49) Glover, P.W. and Walker, E., 2008. Grain-size to effective pore-size transformation derived from electrokinetic theory. *Geophysics*, 74(1), pp. E17-E29.

(50) Wang, F., Yang, K., You, J. and Lei, X., 2019. Analysis of pore size distribution and fractal dimension in tight sandstone with mercury intrusion porosimetry. *Results in Physics*, 13, p.102283.

(51) Yang, F., Ning, Z., & Liu, H. (2014). Fractal characteristics of shales from a shale gas reservoir in the Sichuan Basin, China. *Fuel*, 115, 378-384.

(52) Wang, Q., Yang, S., Han, H., Wang, L., Qian, K. and Pang, J., 2019. Experimental Investigation on the Effects of CO_2 Displacement Methods on Petrophysical Property Changes of Extra-Low Permeability Sandstone Reservoirs near Injection Wells. *Energies*, *12*(2), p. 327.

(53) Wu, H., Zhang, C., Ji, Y., Liu, R., Wu, H., Zhang, Y., Geng, Z., Zhang, Y. and Yang, J., 2018. An improved method of characterizing the pore structure in tight oil reservoirs: Integrated NMR and constant-rate-controlled porosimetry data. *Journal of Petroleum Science and Engineering*, *166*, pp. 778-796.

(54) Revil, A. and Glover, P., 1997. Theory of ionic-surface electrical conduction in porous media. *Physical Review B - Condensed Matter and Materials Physics*, 55(3), pp. 1757-1773.

(55) Revil, A. and Glover, P.W.J., 1998. Nature of surface electrical conductivity in natural sands, sandstones, and clays. *Geophysical Research Letters*, 25(5), pp. 691-694.

(56) Revil, A., Pezard, P.A. and Glover, P.W.J., 1999. Streaming potential in porous media 1. Theory of the zeta potential. *Journal of Geophysical Research: Solid Earth*, 104(B9), pp. 20021-20031.

(57) Uetani, T., 2014. Wettability alteration by asphaltene deposition: A field example. In *Abu Dhabi International Petroleum Exhibition and Conference*. Society of Petroleum Engineers.

(58) Chen, Y., Sari, A., Xie, Q. and Saeedi, A., 2019. Excess H+ Increases Hydrophilicity during CO_2-Assisted Enhanced Oil Recovery in Sandstone Reservoirs. *Energy & fuels*, *33*(2), pp. 814-821.